Feed-forward stimulation of CAMK2 by the oncogenic pseudokinase PEAK1 generates a therapeutically 'actionable' signalling axis in triple negative breast cancer

Xue Yang[1,2], Xiuquan Ma[1,2], David R Croucher[3,4], Elizabeth V. Nguyen[1,2], Kimberley C. Clark[1,2], Changyuan Hu[1,2], Sharissa L Latham[3,4], Tianyue Zhao[1,2], Charles Bayly-Jones[1,2], Viet Chi Bao Nguyen[5], Sung-Young Shin[1,2], Lan K. Nguyen[1,2], Thomas R. Cotton[1,2], Anderly C. Chüeh[1,2], Terry C C Lim Kam Sian[1,2], Margaret M. Stratton[5], Andrew M. Ellisdon[1,2] and Roger J Daly[1,2,#].

[1]Cancer Program, Monash Biomedicine Discovery Institute, Clayton, VIC 3800, Australia.

[2]Department of Biochemistry and Molecular Biology, Monash University, Melbourne, VIC 3800, Australia.

[3]Garvan Institute of Medical Research, Darlinghurst, NSW 2010, Australia.

[4]St Vincent's Clinical School, Faculty of Medicine, UNSW Sydney, Darlinghurst, NSW 2010, Australia.

[5]Department of Biochemistry and Molecular Biology, University of Massachusetts, Amherst, MA 01003, USA

[#]Correspondence: roger.daly@monash.edu

Summary

The PEAK family of pseudokinases, comprising PEAK1-3, are signalling scaffolds that play oncogenic roles in several poor prognosis human cancers, including triple negative breast cancer (TNBC). However, therapeutic targeting of pseudokinases is challenging due to their lack of catalytic activity. To address this, we screened for PEAK1 effectors by affinity purification and mass spectrometry, identifying calcium/calmodulin-dependent protein kinase 2 (CAMK2)D and CAMK2G. PEAK1 promoted CAMK2D/G activation in TNBC cells via a novel feed-forward mechanism involving PEAK1/PLCγ1/Ca^{2+} signalling and direct binding via a consensus CAMK2 interaction motif in the PEAK1 N-terminus. In turn, CAMK2 phosphorylated PEAK1 to enhance association with PEAK2, which is critical for PEAK1 oncogenic signalling. To achieve pharmacologic targeting of PEAK1/CAMK2, we repurposed RA306, a second generation CAMK2 inhibitor under pre-clinical development for treatment of cardiovascular disease. RA306 demonstrated on-target activity against CAMK2 in TNBC cells and inhibited PEAK1-enhanced migration and invasion *in vitro*. Moreover, RA306 significantly attenuated TNBC xenograft growth and blocked metastasis in a manner mirrored by CRISPR-mediated PEAK1 ablation. Overall, these studies establish PEAK1 as a critical cell signalling nexus, identify a novel mechanism for regulation of Ca^{2+} signalling and its integration with tyrosine kinase signals, and identify CAMK2 as a therapeutically 'actionable' target downstream of PEAK1.

Introduction

Pseudokinases play critical roles in normal cellular and developmental processes as well as in human diseases such as cancer, despite lacking the kinase activity of their *bona fide* kinase counterparts. This reflects the ability of pseudokinases to function as allosteric regulators and/or scaffolds that assemble protein signalling complexes[1-3]. Due to their pathological functions, pseudokinases are attracting increasing attention as therapeutic targets[4].

The PEAK family of pseudokinases, comprising PEAK1 (previously known as SgK269), PEAK2 (Pragmin and SgK223) and PEAK3 (C19orf35) share a conserved molecular architecture and sequence homology, and function as scaffolds to mediate and regulate signalling downstream of particular growth factor receptors and integrins[5,6]. PEAK1 is a critical regulator of EGFR signalling, mediating a qualitative shift in signal output over time from mitogenic/survival signalling to that promoting cell migration/invasion[16]. In addition, PEAK1 is overexpressed in a variety of cancers, where it promotes cell proliferation, epithelial-mesenchyme transition, aberrant acinar morphology in 3D culture, xenograft growth and metastasis, and resistance to specific therapies[7-11]. Of particular interest, high PEAK1 expression occurs in triple negative breast cancer (TNBC) and pancreatic cancer[9,10], two cancers associated with poor prognosis and limited targeted therapeutic options. PEAK2 and PEAK3 also enhance cell migration and invasion and are overexpressed in specific malignancies[5,12-16].

All PEAK family members exhibit a C-terminal pseudokinase domain flanked by a split helical dimerization (SHED) domain, and N-terminal extensions of contrasting length that harbour recruitment sites for specific SH2, SH3 and PTB domain-containing effectors. These effectors

include Grb2 (bound by PEAK1 and PEAK3), Shc1 (PEAK1), C-terminal Src kinase (Csk) (PEAK2) and ASAP1, Cbl and PYK2 (PEAK3)[5,6]. An important characteristic of the PEAK family is their ability to form homotypic and heterotypic complexes[5,17]. Dimerization of the PEAKs is mediated by the α-helical SHED domain that forms a highly conserved dimer interface driven by hydrophobic interactions[18,19], while higher order oligomers can also form via pseudokinase domain interfaces[19]. Dimerization is critical to the signalling potential of PEAK scaffolds[5,13,19]. Furthermore, since the repertoire of known interactors differs across this family of scaffolds, heterotypic versus homotypic association acts to diversify signal output[5,17]. For example, PEAK1 requires PEAK2 to efficiently activate Stat3 and promote migration in MCF-10A cells[17,20], while signalling by PEAK3 is modulated both quantitatively and temporally by the presence of PEAK1 and PEAK2[5].

In this study, we addressed how homo- and heterotypic association of PEAK1 and PEAK2 regulates signal output by defining the interactomes of the corresponding dimeric complexes. Amongst the identified binding interactions, the association of PEAK1 with calcium/calmodulin-dependent protein kinase 2 (CAMK2)D and CAMK2G was of particular interest, given the known roles of specific CAMK2 isoforms in many human cancers, including breast cancer, and the therapeutic 'actionability' of these serine/threonine kinases[21,22]. Importantly, we demonstrate potent, feed-forward activation of CAMK2 by PEAK1, highlighting PEAK1 as a critical regulator and integrator of tyrosine kinase and Ca^{2+} signals. In addition, we identify CAMK2D and CAMK2G as novel downstream effectors of PEAK1 in TNBC and 'repurposing' of the second generation CAMK2 inhibitor RA306 as a potential therapeutic strategy against oncogenic PEAK1 signalling in poor prognosis human cancers such as TNBC.

Results

Characterization of dimer-specific interactomes of PEAK1 and PEAK2 by BiCAP

To characterize the interactomes of PEAK1 and PEAK2 homodimers, and the PEAK1/PEAK2 heterodimer, we applied bimolecular complementation affinity purification coupled with tandem mass spectrometry (BiCAP-MS/MS) (Supp. Fig. 1)[23]. Specific dimeric complexes were affinity purified and associated proteins identified by LC-MS/MS (Fig. 1A-C, Supp. Table 1). Grb2, a well-characterized PEAK1 binding partner[9,17] bound the PEAK1 homodimer and PEAK1/PEAK2 heterodimer, but not the PEAK2 homodimer, consistent with our previous results that PEAK1 bridges Grb2 to PEAK2[17]. Two protein phosphatase 1 (PP1) family members, PPP1CA and PPP1CC were previously identified as PEAK1 interactors in a traditional immunoaffinity based-MS/MS screen[20]. However, their selectivity towards PEAK1 versus PEAK2 was unclear. Here, like Grb2, they were identified as interactors of the PEAK1 homodimer and PEAK1/PEAK2 heterodimer, with another PP1 family member, PPP1CB, associating with the PEAK1 homodimer. Of interest given a recent paper reporting a key regulatory role for 14-3-3 proteins in regulating PEAK3 effector recruitment and biological activity[24], multiple 14-3-3 isoforms bound both homodimers and the heterodimer (Supp. Table 1). Further novel interactors identified included the RAC1 guanine nucleotide exchange factor (GEF) FARP1 and the MAPK pathway antagonist SPRY4, which were selective for the PEAK2 homodimer. In addition, Ca^{2+}/calmodulin-dependent protein kinase 2 (CAMK2)D and G associated with the PEAK1 and PEAK2 homodimers and the PEAK1/PEAK2 heterodimer, while CAMK2B was recruited by the PEAK2 homodimer and PEAK1/PEAK2 heterodimer (Figs. 1A-C). Overall, these data provided novel and important insights into the binding

selectivity of PEAK1/2 complexes and identified specific CAMK2 isoforms as novel interactors of these pseudokinase scaffolds.

Characterization of CAMK2 interaction with PEAK1 and PEAK2

To confirm the association of specific CAMK2 family members with PEAK1 and PEAK2, we focused on CAMK2D and CAMK2G, since these kinases associated with all of the homo- and heterotypic PEAK complexes analysed by BiCAP-MS/MS. Interaction of these CAMK2s with endogenous PEAK1 and PEAK2 was interrogated by proximity ligation assays in MDA-MB-231 breast cancer cells (Fig. 1D-F). Using this technique, the interactions between PEAK1 and CAMK2D or G could be detected and were significantly decreased when PEAK1 was knocked down using siRNA (Fig. 1D-E). Similar results were observed for the interactions between PEAK2 and CAMK2D or G (Fig. 1D,F). These data demonstrate that CAMK2D and G interact with both PEAK1 and PEAK2 *in vivo,* at endogenous expression levels.

Regulation of CAMK2 activity by PEAK1

The known overexpression of PEAK1 in breast cancer[8,9] led us to interrogate the functional consequences of PEAK1/CAMK2 interaction. Upon an increase in intracellular Ca^{2+}, binding of Ca^{2+}/calmodulin (CaM) to the CAMK2 regulatory segment leads to release of the regulatory segment from the kinase domain, kinase activation, and phosphorylation of T286 (T287 in CAMK2D and G). In the presence of T286 phosphorylation, the CAMK2 regulatory segment can no longer mediate autoinhibition, and the activity of CAMK2 is Ca^{2+}/CaM autonomous[25]. Knockdown of PEAK1 in MDA-MB-231 TNBC cells did not affect the expression levels of CAMK2D and G but significantly reduced their activation, as determined by phosphorylation

at T287 (Fig. 2A-B). In addition, overexpression of PEAK1 in these cells significantly enhanced activation of these two CAMK2 isoforms (Fig. 2C-D). Positive regulation of CAMK2D/G activity by PEAK1 was also observed in MDA-MB-468 TNBC cells (Supp. Fig. 2). Treatment of MDA-MB-231 cells with BAPTA/AM, a membrane permeable Ca^{2+} chelator which blocks activation of CaM by Ca^{2+} [26], significantly reduced basal CAMK2 T287 phosphorylation and completely blocked the effect of PEAK1 on CAMK2 activation, indicating that PEAK1-mediated CAMK2 activation is Ca^{2+}-dependent (Fig. 2E-F).

In light of this result, we determined whether PEAK1 can modulate Ca^{2+} levels or transients, and thereby indirectly regulate CAMK2 activation. To address this question in the context of a biological endpoint regulated by PEAK1, we undertook real time imaging of an *in vitro* monolayer scratch assay and characterized associated Ca^{2+} signals[27]. This revealed that PEAK1 overexpression significantly enhanced the scratch-induced increase in intracellular Ca^{2+} and also resulted in a more sustained Ca^{2+} increase (Fig. 2G-H). With regard to the mechanism underpinning PEAK1-regulated Ca^{2+} signalling, the known roles of the PEAKs as regulators and/or substrates of specific tyrosine kinases[5,6] led us to determine whether PEAK1 overexpression impacts tyrosine phosphorylation and hence activation of PLCγ1, leading to generation of IP_3 that triggers Ca^{2+} release from intracellular stores[28]. Indeed, PEAK1 knockdown decreased tyrosine phosphorylation of PLCγ1 Y783 (Fig. 2I), while PEAK1 overexpression enhanced PLCγ tyrosine phosphorylation on this site (Fig. 2J). However, given that PEAK1 is a pseudokinase, PLCγ1 phosphorylation must be mediated by a *bona fide* tyrosine kinase acting downstream of PEAK1. Since PEAK1 contains a consensus binding motif for the Src SH2 domain at Y665[11,29] and PLCγ1 is a known substrate of SFKs[30], we hypothesized that SFKs may mediate this role. Supporting this hypothesis, treatment of MDA-

MB-231 TNBC cells with the highly-selective SFK inhibitor eCF506[31] blocked PEAK1-enhanced PLCγ1 tyrosine phosphorylation (Supp. Fig. 3).

Structural requirements for PEAK1/2 interaction with CAMK2

To determine which regions of PEAK1 and PEAK2 mediate interaction with CAMK2D and G, we utilized previously described deletion mutants of PEAK1 and PEAK2[17] that delete the N-terminal region (ΔN-term), N1 α-helix (ΔN1) and a combination of the pseudokinase domain and helices J-M (ΔCterm), as well as a new mutant comprising just the extreme N-terminal region (1-324 amino acids) (N-term) (Fig. 3A). Co-immunoprecipitation of Flag-tagged PEAK1 with endogenous CAMK2D and G could be demonstrated for WT, ΔN1 and ΔCterm PEAK1 but not for the ΔNterm PEAK1 mutant (Fig. 3B). However, the Nterm region alone did not associate with CAMK2D and G, indicating that it is required but not sufficient for interaction with these CAMK2s (Fig. 3B). In addition, since the N1 and Cterm regions are required for PEAK1 to undergo homotypic association and also heterotypic interaction with PEAK2[17], these data also indicated that dimerization is not required for PEAK1 to associate with these CAMK2s. Next, we generated a series of deletion mutants to more narrowly define the CAMK2 binding region on PEAK1 (Fig. 3C). Association with CAMK2D was lost with the Δ261-324 mutant (Fig. 3D). Furthermore, deletion of smaller regions spanning amino acids 261-300 or 301-324 also abolished CAMK2D association (Fig. 3D). Deletion of amino acids 301-324 also markedly reduced CAMK2G association (Fig. 3E).

Although PEAK1 and PEAK2 share similar overall domain architecture, the N-terminal extensions, including the region of PEAK1 required for CAMK2 association (amino acids 261-324), are poorly conserved[17], indicating that the CAMK2 binding mechanism for PEAK2 is

likely to differ. Consistent with this hypothesis, while CAMK2D association with PEAK2 was significantly reduced with the PEAK2 ΔNterm mutant, the greatest effect was observed with the ΔN1 and ΔCterm mutants, which markedly and almost completely abolished association, respectively (Supp. Fig. 4A-C). Since the N1 and Cterm regions are required for PEAK2 to undergo homotypic and heterotypic association[17], these data suggest that PEAK2 interaction with these CAMK2s requires PEAK2 dimerization. Supporting this model, three point mutations in PEAK2 (Supp. Fig. 4A) that abrogate dimerization[19] all led to diminished association with CAMK2D (Supp. Fig. 4D). This contrasts with PEAK1, where the dimerization-impaired ΔN1 and ΔCterm mutants retained association with the CAMK2s. In addition, PEAK1 knockdown did not disrupt association of PEAK2 with CAMK2D (Supp. Fig. 4E), indicating that PEAK2 interaction with CAMK2D is not mediated via PEAK1, consistent with the BiCAP data (Fig. 1B). Taken together, these data highlight contrasting structural requirements for PEAK1 and PEAK2 association with CAMK2, with a greater contribution from a discrete N-terminal region in the case of PEAK1, and a requirement for dimerization in the case of PEAK2.

PEAK1 directly binds CAMK2 via a conserved motif to promote CAMK2 activation and PEAK1 phosphorylation

Since the PEAK1 Δ301-324 mutant was deficient in CAMK2 association (Fig. 3D-E), we determined the effect of this mutant on CAMK2 activation. Interestingly, this mutant was significantly impaired in its ability to activate CAMK2D/G as determined by phosphorylation at T287 (Fig 3F-G), indicating that PEAK1-mediated CAMK2 activation requires association of the two proteins in addition to a Ca^{2+} signal (Fig. 2E-F).

A recent report characterized how CAMK2 interacts with substrate binding partners via a conserved sequence motif in the binding partner, R/K-X-X-ϕ-X-R/K-X-X-S/T-ϕ (where ϕ represents a hydrophobic residue) that binds across a single continuous site on the CAMK2 kinase domain[32]. It also revealed that binding of the conserved CAMK2 interaction motif (CIM) competes with autoinhibition of CAMK2 by the regulatory segment of the kinase domain, explaining the ability of certain substrates, such as GluN2B, to lock CAMK2 in an active conformation[32]. Of note, the Rac GDP/GTP exchange factor TIAM1 exhibits a pseudosubstrate version of the conserved motif (with A rather than S/T), but is still able to bind and promote phosphorylation of itself on other sites[33]. To address whether PEAK1 may interact with CAMK2 via this mechanism, we searched the PEAK1 N-terminal region for the conserved motif. We first constructed a multiple sequence alignment across diverse species and subsequently subjected this to MEME analysis to identify conserved motifs. This analysis revealed that the PEAK1 amino acids 297-307 exhibit close similarity to the canonical binding motif but with an alanine at position 0 (amino acid 306), as observed with TIAM1 (Fig. 4A). Furthermore, the N-terminal region and the binding motif are highly conserved across species (Supp. Fig. 5).

The presence of a CIM between amino acids 297-307 is consistent with disruption of binding by deletion of amino acids 261-300 and 301-324 (Fig. 3D-E) and the failure of the Δ301-324 mutant to activate CAMK2 (Fig 3F-G). To determine whether a synthetic peptide corresponding to the PEAK1 CIM bound CAMK2, we applied isothermal calorimetry. These data revealed a high affinity interaction with a mean K_D of 635 nM (Fig. 4B), comparable to that of the TIAM1 interacting region (1.1 μM)[32]. Modelling of the PEAK1/CAMK2 interaction using AlphaFold predicts (pLDDT 90.7, pTM 0.899) that the PEAK1 CIM interacts across the same surface of the CAMK2 kinase domain as other known interactors[32], with key salt bridges

formed between PEAK1 R303 (-3 position) and R297 (-9) with glutamate residues in CAMK2 (Fig. 4C-F, Supp. Fig. 6). In addition, L301 is accommodated in a hydrophobic pocket of CAMK2 (Fig 4E). We also note the predicted formation of salt bridges by PEAK1 D308, D310 and D311 across the surface of CAMK2 (Fig. 4F). Of note, while this modelling was undertaken with CAMK2A, the binding site is conserved across all CAMK2 isoforms, including CAMK2D and G (Supp. Fig. 6). To test the importance of key residues within the PEAK1 CIM for CAMK2 activation, we generated PEAK1 mutants with alanine substitutions at the R303 (-3), L301 (-5) and R297 (-9) positions (termed AAA) and glutamate substitutions at R303 and R297 (EE). Importantly, both of these mutants lost the ability to activate CAMK2 (Figure 5A-C), supporting the validity of the modelling.

CAMK2 binding to TIAM1 leads to sustained phosphorylation of TIAM1[33]. To determine whether PEAK1 is a substrate for CAMK2, we utilized RA306, a 'next generation' CAMK2 inhibitor developed by Sanofi for chronic cardiovascular indications that is selective for CAMK2D and G over other isoforms[34]. RA306 exhibited 'on-target' activity against CAMK2 in MDA-MB-231 cells (Supp. Fig. 7A) and significantly inhibited PEAK1 serine/threonine phosphorylation (Fig. 6A-B). In addition, recombinant CAMK2 demonstrated *in vitro* kinase activity towards PEAK1 that was detectable using a pAkt substrate antibody that also recognizes the minimal CAMK2 consensus motif for phosphorylation (RXXS/T) or a pSer/Thr antibody (Fig. 6C). Interestingly, PEAK1 phosphorylation was markedly reduced when the PEAK1 AAA and EE CIM mutants were used as substrate, indicating that efficient phosphorylation of PEAK1 by CAMK2 requires interaction of the two proteins via the PEAK1 CIM (Fig. 6C).

CAMK2 phosphorylates PEAK1 to regulate the PEAK1 interactome

In order to characterize the impact of CAMK2-mediated phosphorylation on PEAK1 scaffolding potential, we compared the interactomes of wild-type (WT) PEAK1 and the AAA and EE CIM mutants *in vivo*. We utilized this approach since it more selectively addresses the impact of CAMK2-mediated PEAK1 phosphorylation, while RA306 treatment would exert a more general inhibition of CAMK2-mediated cellular phosphorylation. Binding of the adaptors Crk-L and Grb2, which associate with PEAK1 via SH3 and SH2 domain-mediated interactions, respectively[24,9], was unaffected by the CIM mutations (Supp. Fig. 7B). In contrast, Western blotting of PEAK1 IPs revealed significantly reduced association of 14-3-3 proteins with the two mutants (Supp. Fig. 7C-D). Since 14-3-3 binding to client proteins is classically phosphorylation-dependent, this indicated that impaired CAMK2 activation by the CIM mutants leads to decreased phosphorylation of PEAK1 on 14-3-3 binding sites. Next, we assayed heterotypic association of PEAK1 with PEAK2, a critical determinant of signal output, with PEAK2 binding being required for PEAK1 to promote cell migration and oncogenic signalling[17]. Importantly, whereas heterotypic association of wildtype PEAK1 with PEAK2 in MDA-MB-231 TNBC cells could be readily detected, this was markedly reduced for the CIM mutants (Figure 6D). Overall, these data demonstrate that CAMK2-mediated PEAK1 phosphorylation is a critical regulator of PEAK1-mediated protein-protein interactions and signalling.

PEAK1/CAMK2 signalling is a therapeutically 'actionable' target in TNBC

The finding that CAMK2 and PEAK1 reciprocally regulate led us to interrogate how expression of these proteins is related to breast cancer patient survival. Interestingly, combined high expression of PEAK1 and CAMK2D was significantly associated with poor survival,

while a non-significant trend was detected for the PEAK1/CAMK2G combination (Supp. Fig. 8A-C). Of note, this analysis emphasized the importance of high expression of both PEAK1 and CAMK2D (Supp. Fig. 8B), consistent with a co-activating PEAK1/CAMK2D 'cassette' promoting breast cancer progression.

To characterize the contribution of CAMK2 to PEAK1 oncogenic signalling, we first utilized siRNA-mediated knockdowns. In MDA-MB-231 cells, knockdown of CAMK2D alone had no effect on migration/invasion, while CAMK2G knockdown slightly reduced these responses. However, knockdown of either CAMK2D or G blocked the effect of PEAK1 overexpression on cell migration and invasion (Fig. 7A-B, Supp. Fig. 9A). Second, we exploited the d301-324 PEAK1 mutant, which cannot bind or activate CAMK2 (Fig. 3E-G). This mutant was unable to enhance TNBC cell migration and invasion (Fig. 7C, Supp. Fig. 9B). Third, we applied the selective CAMK2D/G inhibitor RA306[34]. Treatment with this inhibitor blocked PEAK1-promoted migration in both MDA-MB-231 and -468 cells (Fig. 7D, Supp. Fig. 9C-D) and PEAK1-promoted invasion in MDA-MB-231 cells (Supp. Fig. 9E). Overall, these data indicate a requirement for CAMK2 expression and activation, as well as PEAK1/CAMK2 binding, in regulation of cell migration and invasion by PEAK1.

We then evaluated RA306 in an *in vivo* model of TNBC tumour growth and metastasis. Previously, we demonstrated that PEAK1 gene knock-out significantly inhibited growth of MDA-MB-231 TNBC xenografts, as well as experimental metastasis of these cells in a tail vein injection assay[7]. To test RA306, we utilized the highly metastatic variant of this cell line, MDA-MB-231-HM[35], so that we could assay metastatic spread from the primary tumour. In addition, we generated PEAK1-deficient MDA-MB-231-HM cells via CRISPR editing (Supp. Fig. 10A) to compare the effect of RA306 with PEAK1 knock-out and also the combined effect

of these two manipulations. On target activity of RA306 could be detected in the xenografts and PEAK1 ablation also reduced CAMK2 activation (Supp. Fig. 10B-C). RA306 treatment significantly impaired primary tumour growth (Fig. 7E). Importantly, the degree of growth inhibition was similar to that observed upon PEAK1 gene knock-out and combining RA306 with gene knock-out did not enhance this further, strongly suggesting that RA306 treatment and PEAK1 knock-out are targeting the same oncogenic signalling axis (Fig. 7E). Furthermore, we also allowed a separate cohort of primary tumours to grow to the same size, resected them and then monitored metastasis. Strikingly, RA306 blocked metastasis to a similar extent to PEAK1 knock-out (Fig 7F). Overall, these data identify RA306 as a potential therapeutic strategy against the PEAK1/CAMK2 axis in TNBC and potentially other human cancers.

Discussion

The pseudokinase scaffold PEAK1 has emerged as a critical regulator of intracellular signalling, transducing and integrating pleiotropic signals downstream of a variety of growth factor receptors and integrins. For example, PEAK1 promotes Ras activation via Grb2 binding[9], and couples to paxillin regulation at focal adhesions via Crk[7]. In addition, it can indirectly impact Csk and Stat3 via association with PEAK2[17] and ASAP1, PYK2 and Cbl via PEAK3[5]. Our discovery that PEAK1 can also promote Ca^{2+} signals via PLCγ1 and moreover, binds and sustains activation of the Ca^{2+} effector CAMK2 greatly expands the signalling repertoire of this scaffold and cements its role as a fundamental cell signalling nexus. It also identifies PEAK1 as the first member of the kinase superfamily to sustain activation of CAMK2 via direct binding and the first oncoprotein to target CAMK2 via this mechanism. This expansion of the known signalling functions of PEAK1 calls for a re-evaluation of its role in physiological processes linked to CAMK2 signalling including learning and memory,

cardiac function and osteogenic differentiation[21]. As discussed later, it also highlights a potential strategy for therapeutically targeting the oncogenic activity of PEAK1.

Our findings lead to a model whereby PEAK1 enhances and prolongs CAMK2 activation and signalling by two mechanisms that together provide a 'feed-forward' regulatory process for CAMK2 (Supp. Fig. 11). First, PEAK1 overexpression leads to enhanced and more sustained Ca^{2+} signals in cells, reflecting increased tyrosine phosphorylation and hence activation of PLCγ1 which is driven in a SFK-dependent manner. The resulting enhanced Ca^{2+} signal leads to a greater pool of activated CAMK2. Second, PEAK1 binds directly to the Ca^{2+}-activated CAMK2 via the conserved CIM and this has two effects – first, it leads to sustained CAMK2 activation, as determined by T287 phosphorylation, and second, it promotes CAMK2-mediated PEAK1 phosphorylation.

Promotion of CAMK2 T287 phosphorylation and PEAK1 phosphorylation by binding of the PEAK1 CIM to CAMK2 can be explained by a model that incorporates two key characteristics of this enzyme/interactor system - first, the known ability of CAMK2 to form a large holoenzyme comprising 12-14 monomers[36] and second, PEAK1 CIM binding 'locking' CAMK2 in an active state with the αD helix rotated outward[32] (Supp. Fig. 11). In this model, repeated cycles of association/disassociation of one PEAK1 CIM to different CAMK2 subunits within the complex leads to sustained activation of a subset of subunits, allowing continued autophosphorylation on T287, which occurs *in trans*[36], and phosphorylation of PEAK1. However, we accept that alternative, or contributory, mechanisms are conformational changes within the holoenzyme induced by PEAK1 binding to one monomer that promote more widespread enzyme activation and autophosphorylation, and T287 being protected from phosphatase action by PEAK1 binding to CAMK2. In addition, CIM-mediated recruitment of

PEAK1 to one monomer within the Ca^{2+}-activated oligomer leads to phosphorylation of PEAK1 by other activated monomers within the complex. This would be facilitated by the relatively large number of consensus CAMK2 phosphorylation sites present on PEAK1 (41 R/KXXS/T sites in total). Importantly, a precedent for a reciprocally-activating interaction of CAMK2 with a binding partner exhibiting a pseudosubstrate CIM is provided by CAMK2/TIAM1. Here, binding of the TIAM1 CIM to CAMK2 leads to sustained phosphorylation of TIAM1 by CAMK2[33].

An interesting question is the stoichiometry of the resulting PEAK1/CAMK2 complexes. While CAMK2 forms a large holoenzyme complex of 12-14 subunits, PEAK1 can form dimers via the SHED domain and also higher order oligomers via PsK domain interfaces[19]. These properties may facilitate formation of assemblies with CAMK2 oligomers. In addition, the localization of the PEAK1 CIM towards the N-terminus of a largely disordered extension provides considerable flexibility for assembly of large multimeric protein complexes. Interestingly, in contrast to PEAK1, PEAK2 lacks a consensus CIM, and its dimerization potential is essential for CAMK2 association. While the impact of PEAK2 on CAMK2 regulation requires further characterization, one possibility is that PEAK2 contributes to assembly of higher-order complexes of PEAK1/2 with CAMK2.

While PEAK1 is known to be regulated by site-selective tyrosine phosphorylation[9,20,29], our study provides the first demonstration of positive regulation of PEAK1 by serine/threonine phosphorylation. Furthermore, we determine that like tyrosine phosphorylation, this regulates the PEAK1 interactome. In particular, the two PEAK1 CIM mutants, which are poor substrates for CAMK2, exhibit decreased association with PEAK2. This provides one explanation for the role of CAMK2 in PEAK1-enhanced migration, since heterotypic interaction with PEAK2 is

required for this process[17]. Conceivably, CAMK2-mediated phosphorylation may regulate PEAK1 conformation and accessibility of the dimerization and/or oligomerization interfaces. Another protein that exhibits significantly reduced binding to the PEAK1 CIM mutants is 14-3-3. This is consistent with the overlap between the minimal CAMK2 phosphorylation site consensus (R/KXXS/T) and the 14-3-3 mode 1 motif for binding, RXXpS/TXP. In the case of PEAK3, 14-3-3 binding to phosphorylated PEAK3 S69 impairs Grb2 and Crk recruitment to the scaffold, and the PEAK3 S69A mutant exhibits markedly enhanced ability to promote cell migration[24]. With PEAK1, the overall effect of CAMK2-mediated phosphorylation on PEAK1-promoted migration/invasion is positive, so 14-3-3 binding may downregulate binding of negative regulatory factors, and/or increase association with positive ones, such as PEAK2.

Reflecting their role in a variety of disease states, pseudokinases have emerged as potential therapeutic targets, albeit challenging ones given their lack of catalytic activity. Possible therapeutic intervention strategies include the use of small molecule allosteric regulators, therapeutic antibodies for cell surface receptor pseudokinases such as HER3, targeted degradation approaches eg using PROTACs, and pharmacologic modulation of 'actionable' downstream effector pathways[4]. The oncogenic pseudokinase PEAK1 presents a particular conundrum, since it does not bind ATP or GTP, the dimerization interface is relatively large and difficult to target using small molecule drugs, and PEAK1 is an intracellular protein and therefore not accessible by standard therapeutic antibody approaches[6]. However, in this study we identify a novel strategy for targeting PEAK1 signalling that exploits the functional dependency of this kinase on a readily 'actionable' *bona fide* kinase, CAMK2. Importantly, supporting therapeutic targeting of this serine/threonine kinase, CAMK2 isoforms are overexpressed in a variety of human cancers, including breast cancer, where they promote cell proliferation, migration and invasion[21,22]. Expression, as well as activation, of CAMK2 is

significantly higher in lymph node metastases than primary breast cancers, and high expression of the CAMK2 family is associated with worse distant metastasis-free survival in TNBC[22]. In addition, brain metastatic colonization of TNBC is associated with CAMK2 signaling[37].

In general, characterization of the oncogenic role of CAMK2 has been compromised by a poor understanding of regulatory mechanisms, with functional studies often utilizing constitutively active mutants, as well as a reliance on tool compounds for CAMK2 inhibition, such as KN93, that have numerous off-target effects[38]. Our study addresses these issues by identifying the oncogenic pseudokinase PEAK1 as a novel feed-forward activator of CAMK2 and the second generation CAMK2D/G inhibitor RA306 as a suitable targeted agent to block PEAK1/CAMK2 signalling in TNBC and other cancers where PEAK1 is involved, such as pancreatic cancer. Importantly, RA306 avoids central nervous system side-effects and exhibits good oral bioavailability, highlighting its potential for oncology re-purposing[34]. In addition, the identification of a reciprocally-activating PEAK1/CAMK2 complex indicates that these two proteins could be used as predictive biomarkers to guide patient stratification for anti-CAMK2 treatment. Overall, our work identifies an unsuspected interaction across the kinase superfamily with significant implications for our understanding of cell signalling in normal and disease states and precision targeting of PEAK1 and CAMK2.

Acknowledgements

The authors acknowledge the Monash Proteomics and Metabolomics Facility, Monash University, for the provision of mass spectrometry instrumentation, training and technical support, and Monash Micro Imaging for assistance with the calcium imaging experiments. The work was supported by research grants to RJD from the National Health and Medical Research Council of Australia (Ideas Grant 2003599) and Australian Research Council (ARC)

(DP220103638 and DP190103672) and to MMS (NIH R35GM145376). DRC acknowledges fellowship support from the National Breast Cancer Foundation (NBCF Fellowship IIRS-20-032), AME is a Victorian Department of Health and Human Services Victorian Cancer Agency Mid-Career Fellow (MCRF21036) and CB is an ARC DECRA Fellow (DE240100992).

Author Contributions

Conceptualization, RJD; Methodology, XY, XM, DRC, CB, SS, LKN, ACC, MMS, AME, RJD; Investigation, XY, XM, DRC, EVN, KCC, CH, SLL, TZ, CB, VCBN, SS, TCCLKS; Writing – Original Draft, XY, XM, RJD; Writing – Review and Editing, TRC, MMS, AME, RJD; Visualization, XY, TRC, RJD; Funding acquisition, DRC, MMS, CB, AME, RJD; Supervision, XM, RJD; Project administration, RJD.

Declaration of interests

The authors declare that they have no competing interests.

Figure Legends

Figure 1. Identification of specific CAMK2 isoforms as PEAK1/2 interactors via BiCAP-MS/MS. A-C. Results of BiCAP-MS/MS screen. Volcano plots indicate enriched interactors for the PEAK1 homotypic complex (A), PEAK2 homotypic complex (B) and PEAK1/PEAK2 heterotypic complex (C). The known PEAK1 interactor Grb2 and targets of particular interest, including specific CAMK2 family members, are highlighted in red. **D. Western blotting validation of PEAK1 and PEAK2 knockdown.** PEAK1 and PEAK2 were knocked down using siRNA pools, with successful knockdown confirmed by Western blotting. **E-F. Validation of PEAK1/2 association with CAMK2D and CAMK2G by proximity ligation**

assays. Left panels, representative proximity ligation assay (PLA) images from MDA-MB-231 cells for interaction of PEAK1 (E) or PEAK2 (F) with CAMK2D and CAMK2G. Cells were transfected with either si-PEAK1 (E), si-PEAK2 (F) or si-Control. Right panels, quantification of protein interactions in each cell. The data are expressed as dot number divided by cell number. In each condition, more than 50 cells have been counted. Error bars represent the standard error of the mean from n=3 independent experiments. * = $p < 0.05$, ** = $p < 0.01$ by student's t-test.

Figure 2. PEAK1-mediated regulation of CAMK2 activity in triple negative breast cancer cells. A-D. Manipulation of PEAK1 expression modulates CAMK2 activity. PEAK1 was knocked down using a siRNA (A-B) or overexpressed via transient transfection (C-D) in MDA-MB-231 cells and autonomous activation of CAMK2 determined by Western blotting as indicated. Histograms indicate CAMK2 T287 phosphorylation normalized for total CAMK2 expression. **E-F. PEAK1-promoted CAMK2 activation is calcium-dependent.** MDA-MB-231 cells were transfected with a PEAK1 construct in the presence or absence of 10 μM BAPTA-AM. Cell lysates were Western blotted as indicated (E) and CAMK2 activation quantified as above for CAMK2D/G combined (F), with data expressed relative to the DsR (vector)/DMSO control which was arbitrarily set at 1. **G-H. Overexpression of PEAK1 increases intracellular Ca^{2+}.** MDA-MB-231_EcoR cells stably overexpressing PEAK1 were subjected to a Fura-2 AM fluorescence assay for intracellular Ca^{2+} after scratch-induced cell migration. Representative cellular images (G) and corresponding quantification (H) for a time course following the scratch are shown. **I-J. PEAK1 regulates tyrosine phosphorylation of PLCγ1.** MDA-MB-231 cells were transfected with PEAK1 siRNA (I) or a PEAK1 expression vector (J) and then cell lysates were Western blotted as indicated. The histograms indicate Y783-phosphorylated PLCγ1 normalized for total PLCγ1 expression. For all panels, error bars

represent the standard error of the mean from n=3 independent experiments. NS indicates $p > 0.05$, * = $p < 0.05$, ** = $p<0.01$, by ratio paired t-test (B, D, I, J), two-way ANOVA with Tukey's multiple comparisons test (F), or two-way ANOVA with Sidak's multiple comparisons test (H).

Figure 3. Mapping the CAMK2 binding region on PEAK1. A. Schematic structure of PEAK1 and various truncation mutants. WT, wildtype. **B. Association of CAMK2D with specific PEAK1 deletion mutants.** The indicated Flag-tagged PEAK1 deletion mutants were expressed in HEK293T cells. Total cell lysates (TCL) and Flag IPs were subjected to Western blotting as indicated. **C. Schematic representation of various PEAK1 N-terminal deletion mutants.** Deleted regions of PEAK1 are indicated by red crosses. **D-E. Fine structure mapping of N-terminal regions required for the association of PEAK1 with CAMK2D (D) or CAMK2G (E).** Analysis was undertaken as in (B). **F-G. PEAK1 binding to CAMK2 is required for CAMK2 activation.** MDA-MB-231 cells were transfected with WT PEAK1 or the Del 301-324 PEAK1 construct. Cell lysates were Western blotted as indicated (F) and then relative CAMK2 activation, as determined by T287 phosphorylation, quantified (G). Data are expressed relative to vector control which is arbitrarily set at 1. All data in B, D and E are representative of at least 2 independent experiments. In G, error bars represent the standard error of the mean from n=3 independent experiments. NS indicates $p > 0.05$, * = $p < 0.05$ by one-way ANOVA with Tukey's multiple comparisons test.

Figure 4. Characterization of a conserved CAMK2 interaction motif (CIM) on PEAK1. A. Sequence alignment of the PEAK1 CIM with other CAMK2 binding partners. The critical residues for CAMK2 interaction (R297, L301 and R303 in PEAK1) are highlighted in yellow. The canonical motif numbering (A306 being 0) is shown above the alignment. **B.**

Representative ITC measurement of CAMK2 kinase domain binding to PEAK1 CIM peptide. The mean Kd value from n=3 independent experiments is indicated. **C. Comparative modelling of the PEAK1/CAMK2 interaction by AlphaFold.** Surface representation of CAMK2 with PEAK1 amino acids 291-320 shown as ribbon (grey)**.** The orientation is as in Supp Figure 6. CAMK2 is coloured by electrostatic charge. The PEAK1 binding site on CAMK2 is noticeably negative, with key arginine residues of PEAK1 mediating interactions with CAMK2. The N- and C-termini are labelled as N and C, respectively. **D. Surface representation of modelled PEAK1/CAMK2 interaction.** CAMK2 is grey and PEAK1 amino acids 291-320 are purple. **E-F. Focused view of key predicted molecular interactions.** Boxed regions from (D) illustrating salt bridges formed by R303 of PEAK1 and how the negatively charged C-terminal region of the PEAK1 CIM forms salt bridges with multiple aspartic acid residues. The canonical numbering of the PEAK1 motif is shown in white boxes.

Figure 5. The role of the PEAK1 CIM in CAMK2 activation. A-C. Mutational analysis of the PEAK1 CIM. Plasmids encoding WT PEAK1 and the indicated mutants were transfected into MDA-MB-231 cells. Total cell lysates were Western blotted as indicated (A) and then relative CAMK2 activation was quantified (B-C). Data are expressed relative to the vector (DsR) control which was arbitrarily set at 1. NS indicates $p > 0.05$, ** = $p < 0.01$ and **** = $p < 0.0001$ by one-way ANOVA with Dunnett's multiple comparisons test (B, C).

Figure 6. CAMK2 phosphorylates PEAK1 to regulate the PEAK1 interactome. A-B. RA306 inhibits PEAK1 serine/threonine phosphorylation. MDA-MB-231_EcoR cells stably expressing Flag-tagged PEAK1 were treated with RA306 (1 μM) for 24 h and cell lysates

were directly Western blotted or subject to immunoprecipitation with Flag antibody prior to blotting as indicated. Relative serine/threonine phosphorylation of PEAK1, normalized for total PEAK1, is shown in the histogram (B). **C. CAMK2 phosphorylates PEAK1 *in vitro*.** Flag-tagged versions of WT and mutant PEAK1 proteins were expressed in HEK293T cells. PEAK1 proteins were immunoprecipitated using anti-Flag antibody and following washing, immediately treated with SDS-PAGE sample buffer (SB) (no incubation) or incubated in kinase reaction buffer supplemented as indicated at 37ºC for 30 min. Reactions were terminated with SB. Samples were then Western blotted as indicated. The asterisk indicates a background band present in all CAMK2D-incubated samples including the vector control while the arrowhead highlights phosphorylated PEAK1. **D. Impact of CIM mutations on heterotypic association with PEAK2.** Flag-tagged WT PEAK1 or PEAK1 mutants were expressed in MDA-MB-231 cells and association with endogenous PEAK2 assayed by IP/Western. For panel B, * = $p<0.05$ by ratio paired t-test.

Figure 7. Role of CAMK2 in PEAK1-regulated biological endpoints in TNBC models. A. PEAK1 overexpression in combination with CAMK2D and CAMK2G knockdown in MDA-MB-231 cells. Cells were transfected with a PEAK1 plasmid in the presence or absence of siRNA-mediated CAMK2D or CAMK2G knockdown. Cell lysates were Western blotted as indicated. **B. Role of CAMK2D/G in PEAK1-promoted MDA-MB-231 cell migration.** Cells validated in (A) were subjected to a transwell migration assay. **C. Role of CAMK2 activation.** Plasmids expressing WT PEAK1 and the del 301-324 mutant that cannot activate CAMK2 were transiently transfected into MDA-MB-231 cells, and cells were subjected to a transwell migration assay. **D. Effect of the CAMK2 inhibitor RA306.** MDA-MB-231 cells were transfected with a PEAK1 plasmid and subject to transwell migration assays in the presence or absence of RA306. **E. Role of PEAK1/CAMK2 signalling in TNBC xenograft**

growth. Control MDA-MB-231_HM cells (Cas9-control) or PEAK1 KO cells (Cas9-sgPEAK1) in combination with RA306 or vehicle control (captisol) were injected into the mammary fat pad. Left panel, representative whole body bioluminescent imaging (BLI) images from each group at different time points as indicated. Right panel, quantification of xenograft growth. Each treatment group exhibited ≥ 9 mice. **F. Role of PEAK1/CAMK2 signalling in TNBC metastasis.** Control MDA-MB-231_HM cells (Cas9-control) or PEAK1 KO cells (Cas9-sgPEAK1) in combination with RA306 or vehicle control (captisol) were injected into the mammary fat pad. At Day 19 post-injection when the primary tumour from each group reached ~ 100 mm^3, they were resected, and tumour growth at secondary sites was measured. Left panel, representative whole body or *ex vivo* lung BLI images from each group at Day 72 post injection. Right panel, luciferase intensities of tumour metastasis to lung were generated from each group. Each group exhibited n ≥ 8 mice. Error bars represents the standard error of the mean from n=3 independent experiments (B-D) or from the individuals of each group (E & F). NS indicates $p > 0.05$, * = $p < 0.05$, ** = $p < 0.01$, *** = $p < 0.001$ by two-way ANOVA with Tukey's multiple comparisons test (B, D, E), one-way ANOVA with Tukey's multiple comparisons test (C), or one-way ANOVA with Dunnett's multiple comparisons test (F).

Methods

Plasmids and siRNAs

The retroviral expression vector pRetroX-IRES-DsRedExpress (DsR) containing N-terminal HA-tagged and C-terminal FLAG/Myc-tagged PEAK1 as well as its deletion mutants including dNterm, dCterm and dN1, together with the expression vector pMIG containing N-terminal HA-tagged and C-terminal FLAG-tagged PEAK2 as well as PEAK2 site mutants (L955A, L966A, W1382A) were previously generated in our laboratory[17,19]. pRetroX-IRES-DsRedExpress plasmid containing N-terminal Flag-tagged PEAK1 N terminal (residues 1–

324) deleted and other mutants (del 1-260, del 261-300, del 261-324, del 301-324, R297A/L301A/R303A and R297E/R303E) were purchased from GenScript.

pDEST-V1 (Addgene plasmid 73637) and pDEST-V2 (Addgene plasmid 73638) vectors were assembled from various recombinant and synthetic components as described previously[23]. Vectors expressing V1- or V2-labeled fusions of PEAK1 or PEAK2 were generated by recombination cloning from pDONR223-PEAK1 and pDONR223-PEAK2 constructs into pDEST-V1 or pDEST-V2 destination vectors using Gateway LR Clonase enzyme mix (Life Technologies) according to the manufacturer's instructions and verified by sequencing. The expression vector encoding full-length Venus fluorescent protein was a gift from S. Michnick (University of Montreal).

CAMK2A kinase domain (residues 7-274) was cloned into a pET vector containing an N-terminal 6×His followed by a SUMO tag. A D135N mutation was introduced by site-directed mutagenesis.

Sequences of siRNAs were PEAK1 (ON-TARGETplus Human PEAK1 siRNA, cat. LQ-005339-00-0010), PEAK2 (MISSION Human PEAK2 siRNAs, cat. #1: SASI_Hs02_00316033, #2: SASI_Hs02_00316034, #3: SASI_Hs02_00316035, #4: SASI_Hs02_00316036), CAMK2D (siGENOME Human CAMK2D siRNAs, cat. #1: D-004042-02-0002, #2: D-004042-03-0002, #3: D-004042-04-0002, #4: D-004042-05-0002), CAMK2G (siGENOME Human CAMK2G siRNAs, cat. #1: D-004536-01-0005, #2: D-004536-03-0005, #3: D-004536-05-0005, #4: D-004536-06-0005). Negative control siRNA was ON-TARGET plus Non-targeting pool (Dharmacon, D-001810-10-20).

Antibodies

The following antibodies were purchased from Santa Cruz Biotechnology (Dallas, TX): PEAK1 (cat. sc-100403), β-actin (cat. sc-69879) and Pan 14-3-3 (cat. sc-1657). CAMK2D (cat.

ab181052) and CAMK2G (cat. ab201966) were purchased from Abcam. Phospho-Akt Substrate (RXXS*/T*) (cat. 9614), T-CAMK2 (cat. 4436), CAMK2-pT287 (cat. 12716), PLC-γ (cat. 5690S), PLC-γ-pY783 (cat.14008S) were purchased from Cell Signaling Technology. Flag (cat. F1804 and F7425), and α-tubulin (cat. T5168) were purchased from Sigma. The following antibodies were also used: CAMK2D (Genetex, cat. GTX111401), HA (Roche Applied Science, cat. 11867423001). Phospho-Ser/Thr antibody (cat. 612548) was purchased from BD Transduction Laboratories. The custom-made PEAK2 (SgK223) antibody was generated by Cambridge Research Biochemicals Ltd. by standard procedures and described previously[15].

Inhibitors and chemicals

RA306 was custom synthesized by Reagency (cat. RGNCY-0117). The SFK inhibitor eCF506 was obtained from Professor Margaret Frame (Edinburgh Cancer Research Centre). Captisol (cat. A508148) was purchased from AmBeed. BAPTA-AM (cat. A1076) and DMSO (cat. d8418) were purchased from Sigma. Fura-2 AM (cat. ab120873) was purchased from Abcam.

Cell lines and Tissue Culture

HEK293T cells were maintained in Dulbecco's Modified Eagle's Medium (DMEM, Gibco, cat. 1200046) supplemented with 10% (v/v) fetal bovine serum (FBS; Fisher Biotech, cat. S-FBS-US-015). MDA-MB-231 parental cells were obtained from EG&G Mason Research Institute, Worcester, MA. MDA-MB-231 cells stably expressing the murine ecotropic receptor (MDA-MB-231_EcoR) were a kind gift from A/Prof Maija Kohonen-Corish at the Garvan Institute of Medical Research. MDA-MB-468 cells were obtained from the American Type Culture Collection (ATCC). The highly metastatic MDA-MB-231 cell line (MDA-MB-231_HM) was originally established by Prof. Zhou Ou from Fudan University Shanghai Cancer

Center in China. The MDA-MB-231_HM cell line expressing luciferase/mCherry was a kind gift from A/Prof. Erica Sloan at Monash University. In this paper, MDA-MB-231_HM refers to the cell line expressing luciferase/mCherry.

Breast cancer cell lines were maintained in RPMI-1640 medium (Life Technologies, cat. 11875119 and Gibco, cat. 31800-089) supplemented with 10% FBS (Fisher Biotec, cat. S-FBS-US-015), 10 µg/mL Actrapid penfill insulin (Clifford Hallam Healthcare), and 20 mM HEPES (Life Technologies, cat. 15630080). All cell lines were authenticated by short tandem repeat polymorphism, single-nucleotide polymorphism, fingerprint analyses and underwent routine mycoplasma testing by PCR.

Cell Lysis, Immunoprecipitation, and Immunoblotting

Cell lysates for immunoblotting and immunoprecipitation (IP) were prepared using radioimmunoprecipitation (RIPA) buffer and normal lysis buffer (NLB), respectively[39]. For IP of overexpressed Flag- or HA-tagged proteins, cell lysates were incubated with either anti-FLAG M2 affinity-agarose beads (Sigma, cat. A2220) or red anti-HA affinity gel (Sigma, cat. E6779) at 4°C for 2 - 4 h with end-to-end rotation. After the incubation, the beads were washed extensively with ice-cold lysis buffer, the immune complexes were eluted with SDS-PAGE loading buffer, and subjected to Western blotting analysis, which was performed following SDS-polyacrylamide gel electrophoresis using 5% stacking gels and 8%, 10% or 12% separating gels.

Generation of PEAK1 knock-out cells

Stable MDA-MB-231_HM PEAK1 knockout cells were generated using the Synthego Immortalized Cell Nucleofection Protocol as per manufacturer's instructions (Synthego). Briefly, ribonucleoprotein (RNP) complexes were assembled by combining Cas9 2NLS

(Synthego), human PEAK1 sgRNA (Gene Knockout Kit v2, Synthego) and Nucleofector SolutionTM L + supplement (Synthego) and incubating at room temperature for 10 mins. RNP complexes were combined with cells in NucleocuvetteTM strips immediately prior to electroporation. Cells were electroporated using the 4D-X Core unit (Lonza) using setting CH-125. Cells were immediately resuspended in normal culture medium following electroporation. Cell lysates were collected 72h post-electroporation to confirm PEAK1 knockout efficiency by Western blot.

Transfections

SMARTpool siRNA or individual siRNA duplexes were applied to cells using DharmaFECT (Dharmacon, Lafayette, CO) transfection reagent according to the manufacturer's instructions. Plasmid transfections were performed using Lipofectamine 3000 (Invitrogen) according to the manufacturer's instructions.

BiCAP and LC-MS/MS

This was performed as previously described[23]. Briefly, HEK293T cells were transfected with the appropriate BiCAP constructs. Cells were lysed with ice-cold lysis buffer comprising 50 mM Tris (pH 7.4), 150 mM NaCl, 1 mM EDTA, 1% (v/v) TritonX-100 supplemented with fresh EDTA-free protease inhibitor cocktail and 0.2 mM sodium orthovanadate. Samples were cleared by centrifugation at 18,000 g for 10 min at 4 °C to remove cellular debris. Total protein concentration was determined by Bradford assay using Bio-Rad Protein Assay Dye Reagent Concentrate (Bio-Rad Laboratories) according to the manufacturer's instructions. To purify BiCAP dimers (or Venus alone as a negative control for nonspecific interactions), 1 mg of total lysate (in triplicate) was incubated with 35 µl of GFP-Trap_A agarose beads slurry (ChromoTek GmbH) for 2 h at 4°C with end-to-end rotation. Beads were extensively washed

with wash buffer [10 mM Tris (pH 7.5), 150 mM NaCl, 0.5 mM EDTA] and subjected to on-bead digestion with trypsin, and the resulting peptides were analyzed by LC-MS/MS on a Q-Exactive MS instrument (Thermo Scientific). Peptides were separated by nano-LC using an UltiMate 3000 high performance liquid chromatography and autosampler system (Dionex, Sunnyvale, CA). Samples were subjected to positive nanoflow electrospray analysis in data-independent acquisition mode (250 nl/min for 30 min).

Data Processing

Raw files were processed with MaxQuant (version 1.5.2.8)[40]. MaxLFQ, MaxQuant's label-free quantification (LFQ) algorithm was used to calculate protein intensity profiles across samples[41], including the "match between runs" option. Perseus (version 2019) was used to normalize the data and impute for missing values[42]. Candidate interacting proteins were defined by applying the following criteria: p value <0.05 by two-tailed *t*-test and a log2 fold change of ≥ 1.5 against the Venus control.

Protein expression and purification

CAMK2A D135N kinase domain was recombinantly expressed in BL21(DE3) cells (Millipore) as previously described[32]. Protein expression was induced for ~6 h by 1 mM isopropyl β-a-D-1-thiogalactopyranoside (IPTG; GoldBio) in an 18 °C shaker. Cell pellets were resuspended and lysed in Buffer A [25 mM Tris pH 8.5, 50 mM KCl, 40 mM imidazole, 10% glycerol] with protease inhibitor mixture [0.2 mM AEBSF, 5.0 μM leupeptin, 1 μg/ml pepstatin, 1 μg/ml aprotinin, 0.1 mg/ml trypsin inhibitor, 0.5 mM benzamidine] and DNase (1 μg/ml; Sigma). Protein purification was performed using an ÄKTA pure chromatography system at 4 °C. After pelleting the cell debris, clarified cell lysate was loaded onto two 5 mL HisTrap FF Ni-NTA Sepharose columns (GE) and eluted with a combination of 50% buffer A

and 50% buffer B [25 mM Tris-HCl pH 8.5, 150 mM KCl, 1 M imidazole, 10% glycerol] for a final concentration of 0.5 M imidazole. Protein was desalted using a HiPrep 26/10 desalting column (GE), and His-SUMO tags were cleaved with Ulp1 protease overnight at 4 °C in buffer C [25 mM Tris-HCl pH 8.5, 40 mM KCl, 40 mM imidazole, 2 mM tris(2-carboxyethyl) phosphine (TCEP), 10% glycerol]. Cleaved tags were separated by a subtractive Ni-NTA step followed by an anion exchange step performed with a 5-ml HiTrap Q-FF (GE) and protein was eluted with a KCl gradient. Eluted proteins were concentrated and further purified in gel filtration buffer [25 mM tris-HCl pH 8.0, 150 mM KCl, 1 mM TCEP, 10% glycerol] using a Superdex 75 10/300 GL size exclusion column (GE). Pure fractions were then concentrated, aliquoted, flash-frozen in liquid nitrogen, and stored at −80 °C until further use.

Peptide synthesis

The PEAK1 peptide used for ITC was synthesized to >95% purity with acetylation at the N-terminus and amidation at the C-terminus (Genscript). The peptide sequence was as follows: KKWNTIPLRNKSLQRICAVDYDDSYD.

Isothermal titration calorimetry

ITC data were obtained using a Malvern Auto-iTC200 calorimeter (UMass Amherst). Peptide was dissolved in gel filtration buffer with 6% v/v DMSO and concentration was determined using ε280 = 8370 M-1cm-1. CAMK2 kinase domain was diluted in gel filtration buffer with 5.6% v/v DMSO and concentration was determined with ε280 = 43850 M-1cm-1. Titrations were performed with the peptide as the titrant. Blank titrations were performed by injecting the peptide into gel filtration buffer. All titrations were performed at 20 °C using the standard 19-injection method where one injection of 0.4 µL is followed by 18 x 2 µL injections with 150 s between injections. The stir speed was set to 750 rpm, and the reference power was set to 10.

Data were buffer-subtracted and analyzed using MicroCal ITC Origin add-on dissociation model v1.00 using the one-site fitting model.

Comparative modelling of PEAK1(291-320):CAMK2

Several candidate structural models of PEAK1(291-320):CAMK2 were generated by AlphaFold-Multimer[43,44] (v3) using the ColabFold[45] (v1.5.1) community implementation. Multiple sequence alignments and template searches were performed by MMseqs[43] and HHsearch using default settings. Custom templates of CAMK2 in complex with known tight binders were required to achieve models with acceptable metrics of pLTTD and pTM scores. These interactions were manually curated from crystal structures determined by Özden et al[32] (crystal symmetry mates were discarded). Six recycle rounds were conducted and final models were ranked according to pTMscore. The best scoring models were relaxed with Amber[46] to minimize steric clashes.

Cross species multiple sequence alignment of PEAK1 N-terminus

To generate a multiple sequence alignment, two rounds of PSI-BLAST[47] were performed against the non-redundant clustered database[48] (to increase taxonomic depth) using human PEAK1 as a query sequence. A cutoff of expectation value of $1x10^{-3}$ was used to select sequences for subsequent rounds and alignment. Finally, the top 50 and top 250 sequences (sorted by expectation value) were subjected to alignment in Clustal Omega[49,50]. The full sequence range for the top 250 sequences was subjected to a MEME[51] search to identify consensus motifs.

Proximity ligation assay (PLA)

PLA was performed to detect protein-protein interactions in MDA-MB-231 cells using

Duolink™ In Situ Red Starter Kit (Sigma, cat. DUO92101). All the reagents, including probes, detection reagents and wash buffers were provided in this kit. On day 1, $6x10^4$ cells were seeded per well in a 48-well plate and incubated at 37 °C overnight. On day 2, cells were gently washed 3 times with 1x phosphate-buffered saline [PBS; NaCl (136 mM), KCl (2.6 mM), Na2HPO4 (10 mM), KH2PO4 (1.76 mM)], and then fixed in 4% (v/v) paraformaldehyde (VWR, cat. ALFA43368.9M) for 30 min on ice. Following that, cells were washed with 1xPBS again and permeabilized with 0.2% Triton X-100 (Sigma, cat. T8787) for 3 min at room temperature. After another 1xPBS washing step, cells were incubated with blocking solution for 30 min at 37 °C, following which, cells were incubated with two primary antibodies from different species against the targeted proteins overnight at 4 °C. On day 3, cells were washed with 1x Tris buffered saline (TBS) solution with the detergent Tween-20 [TBS-T; Tris base (50 mM), NaCl (150 mM), pH 7.6, Tween-20 (0.01% v/v)], then PLA probes were added to the cells and incubated for 60 min at 37 °C. Following ligation and amplification steps, samples were mounted with Mounting Medium with DAPI (Invitrogen, cat. P-36931). Cells were photographed using a confocal microscope and dot numbers were analyzed using ImageJ software (Version 1.52).

Calcium Assay

MDA-MB-231_EcoR cells were subjected to retroviral-mediated transduction with DsR empty vector or WT PEAK1 vector as previously described[52]. The cells were seeded in a 24-well plate with a black wall/clear bottom and allowed to adhere overnight. The next day, the cells were washed twice with Hanks and Hepes buffer (HHBS) solution, followed by the addition of starvation growth medium (RPMI-1640 medium supplemented with 0.4% FBS, 10 µg/mL Actrapid penfill insulin and 20 mM HEPES) containing 5 µM Fluo-2 AM. After 1 h incubation at 37°C, the cells were again washed with HHBS solution, and the dye-loaded solution was

replaced with the starvation growth medium. Subsequently, a straight wound was made across the cell monolayer in each well using a 20 µl pipette tip. Finally, cellular fluorescence was monitored over time using a Leica DMi8 fluorescence microscope equipped with a FITC filter (excitation wavelength 460-500 nm and emission wavelength 512-542 nm) and environmental chamber set at 37C with 5% CO2 supplied.

Transwell Migration/Invasion Assay

Transwell migration and invasion assays were essentially as previously described[53]. Transwell migration chambers with 8-µm pores were purchased from Corning (cat. CLS3464-48EA) and MERCK Millipore (cat. MCEP24H48). Matrigel invasion chambers pre-coated with Matrigel were purchased from Corning (cat. 354483). Prior to seeding, cells were treated with mitomycin C at 10µg/ml for 1 h to prevent cell division.

In vitro kinase assay

HEK293T cells were transiently transfected with plasmids encoding wildtype PEAK1 or the CAMK2-interaction motif mutants. Cell lysates were prepared using RIPA buffer[39] supplemented with 12.5 mM β-glycerol phosphate. Cell lysates were then incubated with anti-FLAG M2 affinity-agarose beads (Sigma, cat. A2220) at 4°C for 2 h with end-to-end rotation. After the incubation, the beads were washed extensively with ice-cold RIPA buffer and kinase reaction buffer [Tris (pH 7.5) 40 mM, $MgCl_2$ 10 mM, $CaCl_2$ 0.5 mM]. After the last wash, beads were incubated in kinase reaction buffer supplemented with 100 ng recombinant CAMK2D (Invitrogen, cat. PV3373), 100 µM recombinant calmodulin (Enzo, cat. BML-SE325-0001) and 2 mM Adenosine 5'-triphosphate (ATP) disodium salt hydrate (Sigma-Aldrich, cat. A1852-1VL) for 30 min at 37 ºC. Following incubation, the immune complexes were eluted with SDS-PAGE loading buffer and subjected to Western blotting analysis.

Animal Studies

All procedures involving mice were conducted in accordance with National Health and Medical Research Council (NHMRC) regulations on the use and care of experimental animals and the study protocol approved by the Monash University Animal Ethics Committee.

Power calculations performed indicated group sizes of n = 8 per treatment group were required to detect a significant difference in tumor growth inhibition of 50% between treated and control (significance level: 0.05; power: 90%). All *in vivo* experiments were performed with 6-week-old female BALB/c athymic nude mice obtained from the Animal Resources Centre (Canning Vale, Australia) and housed in sterile conditions at Monash Animal Research Platform. Throughout the study, each cage was randomly assigned to the experimental groups without considering any other variable. Mice were randomly divided into four equal groups, cas9-control cells with captisol (control), cas9-control cells with RA306, cas9-sgPEAK1 cells with captisol and cas9-sgPEAK1 cells with RA306.

Xenograft model

Mice (n=40) were injected with 2×10^5 MDA-MB-231_HM Cas9 control or sgPEAK1 stable knockdown cells suspended in 20µl PBS into the fourth mammary fat pad. One day post-injection, RA306 (30mg/kg) or captisol-only control was administered via daily oral gavage until the end of the experiment. To measure tumour burden, mice were injected with luciferin (150 mg/kg) by an intraperitoneal route. Tumour burden was measured weekly using the AMI-HTX imaging system (Spectral Instruments Imaging). Results are presented as mean +/- SEM of total BLI signal (photons/s).

Tumour metastasis model

Mice (n=40) were injected with 2×10^5 MDA-MB-231_HM Cas9 control or sgPEAK1 stable knockdown cells suspended in 20µl PBS into the fourth mammary fat pad. One day post-injection, RA306 (30mg/kg) or captisol-only control was administered via daily oral gavage until the end of the experiment. When the primary tumours from each group reached ~ 100 mm^3 in size, they were resected. Tumour metastasis to secondary sites was then measured weekly using the AMI-HTX imaging system (Spectral Instruments Imaging). Organs were dissected immediately following the final BLI image and re-imaged in the AMI-HTX ex vivo to allow for direct measurement of organ-specific tumour burden via BLI. Results are presented as mean tumour luciferase intensities +/- SEM of total BLI signal (photons/s).

Tumour tissue homogenization

Following dissection at the experimental endpoint, tumour tissues were transferred immediately to dry ice. Tumour tissues were cut into small pieces and added to a 1.5ml tube containing RIPA buffer and Zirconia tissue disruption beads (Research Products International, cat. 9835) then homogenized for 10s at low speed and 30s at high speed at room temperature. To prepare samples for Western blotting, homogenized samples were centrifuged for 20 min at 20,000g at 4°C. The supernatant was then collected and the protein concentration determined using either Bradford Ultra Protein Assay Reagent (Expedeon, cat. EP-BFU05L) or Pierce TM BCA Protein Assay Reagents (Thermo Scientific, cat. 23225). The protein concentration of each sample was subsequently adjusted using RIPA buffer, and SDS-PAGE loading buffer was added prior to Western blotting analysis.

Survival Analysis

For survival analysis, mRNA expression, mutation profile and associated overall survival data from 2509 breast cancer patients as part of the METABRIC trial [54] were downloaded from the

cBioPortal for Cancer Genomics portal (https://www.cbioportal.org/). Breast cancer patients were divided and classified into three main groups each having either low, or medium, or high expression of *CAMK2D, CAMK2G* or *PEAK1*, individually. Main groups were then further categorised into four sub-groups exhibiting different combined expression patterns: *i) CAMK2D* and *PEAK1* both high, *ii) CAMK2D* and *PEAK1* both low, *iii) CAMK2G* and *PEAK1* both high, *iv) CAMK2G* and *PEAK1* both low, *v) CAMK2D* low and *PEAK1* high, *vi) CAMK2D* high and *PEAK1* low. Survival analyses comparing overall survival between these sub-groups were subsequently performed using a Log-rank test (with $p < 0.05$ considered significant). The Log-rank test statistics and survival curves were generated using Kaplan-Meier estimate and implemented using the Logrank package[54] in MATLAB 2023a.

Statistical analyses

Experimental data were subject to appropriate statistical analyses as detailed in the corresponding figure legends.

Data availability

The mass spectrometry proteomics data for the spectral library and DIA analysis have been deposited to the ProteomeXchange Consortium via the PRIDE[55] partner repository with the dataset identifier PXD044872. Raw data generated in this study are available upon request from the corresponding author.

Supplementary Information Titles and Legends

Supp.Table 1. BiCAP-MS/MS data for PEAK dimer-specific interactomes.

Supp. Figure 1. Schematic strategy of BiCAP-MS/MS screen.

Supp. Figure 2. Manipulation of PEAK1 expression modulates CAMK2 activity in MDA-MB-468 cells.

Supp. Figure 3. Effect of SFK inhibitor eCF506 on PLCγ1 Y783 phosphorylation.

Supp. Figure 4. Determination of the structural requirements for CAMK2 interaction with PEAK2.

Supp. Figure 5. Sequence alignment of the PEAK1 CIM motif across diverse species.

Supp. Figure 6. Comparative modelling analysis by AlphaFold (to accompany Figure 4C-F).

Supp. Figure 7. Role of CAMK2 in regulating PEAK1 phosphorylation and the PEAK1 interactome.

Supp. Figure 8. Association of PEAK1 and CAMK2 expression with breast cancer patient survival.

Supp. Figure 9. Role of CAMK2 in PEAK1-regulated biological endpoints in TNBC models.

Supp. Figure 10. Genetic or pharmacological targeting of the PEAK1/CAMK2 axis reduces TNBC development *in vivo*.

Supp. Figure 11. Schematic model for feedforward regulation of CAMK2 by PEAK1.

References

1. Manning, G., Whyte, D.B., Martinez, R., Hunter, T., and Sudarsanam, S. (2002). The protein kinase complement of the human genome. Science *298*, 1912-1934. 10.1126/science.1075762.
2. Reiterer, V., Eyers, P.A., and Farhan, H. (2014). Day of the dead: pseudokinases and pseudophosphatases in physiology and disease. Trends in cell biology *24*, 489-505. 10.1016/j.tcb.2014.03.008.
3. Zeqiraj, E., and van Aalten, D.M. (2010). Pseudokinases-remnants of evolution or key allosteric regulators? Current opinion in structural biology *20*, 772-781. 10.1016/j.sbi.2010.10.001.
4. Kung, J.E., and Jura, N. (2019). Prospects for pharmacological targeting of pseudokinases. Nat Rev Drug Discov *18*, 501-526. 10.1038/s41573-019-0018-3.
5. Hou, J., Nguyen, E.V., Surudoi, M., Roy, M.J., Patel, O., Lucet, I.S., Ma, X., and Daly, R.J. (2022). Distinct PEAK3 interactors and outputs expand the signaling potential of the PEAK pseudokinase family. Sci Signal *15*, eabj3554. 10.1126/scisignal.abj3554.

6. Patel, O., Roy, M.J., Murphy, J.M., and Lucet, I.S. (2020). The PEAK family of pseudokinases, their role in cell signalling and cancer. FEBS J *287*, 4183-4197. 10.1111/febs.15087.
7. Abu-Thuraia, A., Goyette, M.-A., Boulais, J., Delliaux, C., Apcher, C., Schott, C., Chidiac, R., Bagci, H., Thibault, M.-P., and Davidson, D. (2020). AXL confers cell migration and invasion by hijacking a PEAK1-regulated focal adhesion protein network. Nature communications *11*, 1-20.
8. Agajanian, M., Campeau, A., Hoover, M., Hou, A., Brambilla, D., Kim, S.L., Klemke, R.L., and Kelber, J.A. (2015). PEAK1 Acts as a Molecular Switch to Regulate Context-Dependent TGFbeta Responses in Breast Cancer. PLoS One *10*, e0135748. 10.1371/journal.pone.0135748.
9. Croucher, D.R., Hochgrafe, F., Zhang, L., Liu, L., Lyons, R.J., Rickwood, D., Tactacan, C.M., Browne, B.C., Ali, N., Chan, H., et al. (2013). Involvement of Lyn and the atypical kinase SgK269/PEAK1 in a basal breast cancer signaling pathway. Cancer Res *73*, 1969-1980. 10.1158/0008-5472.CAN-12-1472.
10. Kelber, J.A., Reno, T., Kaushal, S., Metildi, C., Wright, T., Stoletov, K., Weems, J.M., Park, F.D., Mose, E., Wang, Y., et al. (2012). KRas induces a Src/PEAK1/ErbB2 kinase amplification loop that drives metastatic growth and therapy resistance in pancreatic cancer. Cancer Res *72*, 2554-2564. 10.1158/0008-5472.CAN-11-3552.
11. Wang, Y., Kelber, J.A., Tran Cao, H.S., Cantin, G.T., Lin, R., Wang, W., Kaushal, S., Bristow, J.M., Edgington, T.S., Hoffman, R.M., et al. (2010). Pseudopodium-enriched atypical kinase 1 regulates the cytoskeleton and cancer progression [corrected]. Proc Natl Acad Sci U S A *107*, 10920-10925. 10.1073/pnas.0914776107.
12. Leroy, C., Fialin, C., Sirvent, A., Simon, V., Urbach, S., Poncet, J., Robert, B., Jouin, P., and Roche, S. (2009). Quantitative phosphoproteomics reveals a cluster of tyrosine kinases that mediates SRC invasive activity in advanced colon carcinoma cells. Cancer Res *69*, 2279-2286. 10.1158/0008-5472.CAN-08-2354.
13. Ounoughene, Y., Fourgous, E., Boublik, Y., Saland, E., Guiraud, N., Recher, C., Urbach, S., Fort, P., Sarry, J.E., Fesquet, D., and Roche, S. (2021). SHED-Dependent Oncogenic Signaling of the PEAK3 Pseudo-Kinase. Cancers (Basel) *13*. 10.3390/cancers13246344.
14. Senda, Y., Murata-Kamiya, N., and Hatakeyama, M. (2016). C-terminal Src kinase-mediated EPIYA phosphorylation of Pragmin creates a feed-forward C-terminal Src kinase activation loop that promotes cell motility. Cancer Sci *107*, 972-980. 10.1111/cas.12962.
15. Tactacan, C.M., Phua, Y.W., Liu, L., Zhang, L., Humphrey, E.S., Cowley, M., Pinese, M., Biankin, A.V., and Daly, R.J. (2015). The pseudokinase SgK223 promotes invasion of pancreatic ductal epithelial cells through JAK1/Stat3 signaling. Mol Cancer *14*, 139. 10.1186/s12943-015-0412-3.
16. Lecointre, C., Fourgous, E., Montarras, I., Kerneur, C., Simon, V., Boublik, Y., Bonenfant, D., Robert, B., Martineau, P., and Roche, S. (2022). Oncogenic Signalling of PEAK2 Pseudokinase in Colon Cancer. Cancers (Basel) *14*. 10.3390/cancers14122981.
17. Liu, L., Phua, Y.W., Lee, R.S., Ma, X., Jenkins, Y., Novy, K., Humphrey, E.S., Chan, H., Shearer, R., Ong, P.C., et al. (2016). Homo- and Heterotypic Association Regulates Signaling by the SgK269/PEAK1 and SgK223 Pseudokinases. J Biol Chem *291*, 21571-21583. 10.1074/jbc.M116.748897.
18. Ha, B.H., and Boggon, T.J. (2018). The crystal structure of pseudokinase PEAK1 (Sugen kinase 269) reveals an unusual catalytic cleft and a novel mode of kinase fold dimerization. J Biol Chem *293*, 1642-1650. 10.1074/jbc.RA117.000751.

19. Patel, O., Griffin, M.D.W., Panjikar, S., Dai, W., Ma, X., Chan, H., Zheng, C., Kropp, A., Murphy, J.M., Daly, R.J., and Lucet, I.S. (2017). Structure of SgK223 pseudokinase reveals novel mechanisms of homotypic and heterotypic association. Nat Commun *8*, 1157. 10.1038/s41467-017-01279-9.
20. Zheng, Y., Zhang, C., Croucher, D.R., Soliman, M.A., St-Denis, N., Pasculescu, A., Taylor, L., Tate, S.A., Hardy, W.R., Colwill, K., et al. (2013). Temporal regulation of EGF signalling networks by the scaffold protein Shc1. Nature *499*, 166-171. 10.1038/nature12308.
21. Brzozowski, J.S., and Skelding, K.A. (2019). The Multi-Functional Calcium/Calmodulin Stimulated Protein Kinase (CaMK) Family: Emerging Targets for Anti-Cancer Therapeutic Intervention. Pharmaceuticals (Basel) *12*. 10.3390/ph12010008.
22. Chi, M., Evans, H., Gilchrist, J., Mayhew, J., Hoffman, A., Pearsall, E.A., Jankowski, H., Brzozowski, J.S., and Skelding, K.A. (2016). Phosphorylation of calcium/calmodulin-stimulated protein kinase II at T286 enhances invasion and migration of human breast cancer cells. Sci Rep *6*, 33132. 10.1038/srep33132.
23. Croucher, D.R., Iconomou, M., Hastings, J.F., Kennedy, S.P., Han, J.Z., Shearer, R.F., McKenna, J., Wan, A., Lau, J., Aparicio, S., and Saunders, D.N. (2016). Bimolecular complementation affinity purification (BiCAP) reveals dimer-specific protein interactions for ERBB2 dimers. Sci Signal *9*, ra69. 10.1126/scisignal.aaf0793.
24. Roy, M.J., Surudoi, M.G., Kropp, A., Hou, J., Dai, W., Hardy, J.M., Liang, L.Y., Cotton, T.R., Lechtenberg, B.C., Dite, T.A., et al. (2023). Structural mapping of PEAK pseudokinase interactions identifies 14-3-3 as a molecular switch for PEAK3 signaling. Nat Commun *14*, 3542. 10.1038/s41467-023-38869-9.
25. Bhattacharyya, M., Karandur, D., and Kuriyan, J. (2020). Structural Insights into the Regulation of Ca(2+)/Calmodulin-Dependent Protein Kinase II (CaMKII) ——— Review. Cold Spring Harb Perspect Biol *12*. 10.1101/cshperspect.a035147.
26. Tsien, R.Y. (1981). A non-disruptive technique for loading calcium buffers and indicators into cells. Nature *290*, 527-528. 10.1038/290527a0.
27. Pratt, S.J.P., Hernandez-Ochoa, E.O., Lee, R.M., Ory, E.C., Lyons, J.S., Joca, H.C., Johnson, A., Thompson, K., Bailey, P., Lee, C.J., et al. (2018). Real-time scratch assay reveals mechanisms of early calcium signaling in breast cancer cells in response to wounding. Oncotarget *9*, 25008-25024. 10.18632/oncotarget.25186.
28. Mandal, S., Bandyopadhyay, S., Tyagi, K., and Roy, A. (2021). Recent advances in understanding the molecular role of phosphoinositide-specific phospholipase C gamma 1 as an emerging onco-driver and novel therapeutic target in human carcinogenesis. Biochim Biophys Acta Rev Cancer *1876*, 188619. 10.1016/j.bbcan.2021.188619.
29. Bristow, J.M., Reno, T.A., Jo, M., Gonias, S.L., and Klemke, R.L. (2013). Dynamic phosphorylation of tyrosine 665 in pseudopodium-enriched atypical kinase 1 (PEAK1) is essential for the regulation of cell migration and focal adhesion turnover. J Biol Chem *288*, 123-131. 10.1074/jbc.M112.410910.
30. Jones, N.P., Peak, J., Brader, S., Eccles, S.A., and Katan, M. (2005). PLCgamma1 is essential for early events in integrin signalling required for cell motility. J Cell Sci *118*, 2695-2706. 10.1242/jcs.02374.
31. Temps, C., Lietha, D., Webb, E.R., Li, X.F., Dawson, J.C., Muir, M., Macleod, K.G., Valero, T., Munro, A.F., Contreras-Montoya, R., et al. (2021). A Conformation Selective Mode of Inhibiting SRC Improves Drug Efficacy and Tolerability. Cancer Res *81*, 5438-5450. 10.1158/0008-5472.CAN-21-0613.
32. Ozden, C., Sloutsky, R., Mitsugi, T., Santos, N., Agnello, E., Gaubitz, C., Foster, J., Lapinskas, E., Esposito, E.A., Saneyoshi, T., et al. (2022). CaMKII binds both

substrates and activators at the active site. Cell Rep *40*, 111064. 10.1016/j.celrep.2022.111064.
33. Saneyoshi, T., Matsuno, H., Suzuki, A., Murakoshi, H., Hedrick, N.G., Agnello, E., O'Connell, R., Stratton, M.M., Yasuda, R., and Hayashi, Y. (2019). Reciprocal Activation within a Kinase-Effector Complex Underlying Persistence of Structural LTP. Neuron *102*, 1199-1210 e1196. 10.1016/j.neuron.2019.04.012.
34. Beauverger, P., Ozoux, M.L., Begis, G., Glenat, V., Briand, V., Philippo, M.C., Daveu, C., Tavares, G., Roy, S., Corbier, A., et al. (2020). Reversion of cardiac dysfunction by a novel orally available calcium/calmodulin-dependent protein kinase II inhibitor, RA306, in a genetic model of dilated cardiomyopathy. Cardiovascular research *116*, 329-338. 10.1093/cvr/cvz097.
35. Yang, X., Cruz, M.I., Nguyen, E.V., Huang, C., Schittenhelm, R.B., Luu, J., Cowley, K.J., Shin, S.Y., Nguyen, L.K., Lim Kam Sian, T.C.C., et al. (2023). The pseudokinase NRBP1 activates Rac1/Cdc42 via P-Rex1 to drive oncogenic signalling in triple-negative breast cancer. Oncogene *42*, 833-847. 10.1038/s41388-023-02594-w.
36. Bhattacharyya, M., Karandur, D., and Kuriyan, J. (2020). Structural Insights into the Regulation of Ca(2+)/Calmodulin-Dependent Protein Kinase II (CaMKII). Cold Spring Harb Perspect Biol *12*. 10.1101/cshperspect.a035147.
37. Ren, D., Zhu, X., Kong, R., Zhao, Z., Sheng, J., Wang, J., Xu, X., Liu, J., Cui, K., Zhang, X.H., et al. (2018). Targeting Brain-Adaptive Cancer Stem Cells Prohibits Brain Metastatic Colonization of Triple-Negative Breast Cancer. Cancer Res *78*, 2052-2064. 10.1158/0008-5472.CAN-17-2994.
38. Pellicena, P., and Schulman, H. (2014). CaMKII inhibitors: from research tools to therapeutic agents. Front Pharmacol *5*, 21. 10.3389/fphar.2014.00021.
39. Brummer, T., Schramek, D., Hayes, V.M., Bennett, H.L., Caldon, C.E., Musgrove, E.A., and Daly, R.J. (2006). Increased proliferation and altered growth factor dependence of human mammary epithelial cells overexpressing the Gab2 docking protein. Journal of Biological Chemistry *281*, 626-637.
40. Cox, J., and Mann, M. (2008). MaxQuant enables high peptide identification rates, individualized p.p.b.-range mass accuracies and proteome-wide protein quantification. Nature biotechnology *26*, 1367-1372. 10.1038/nbt.1511.
41. Cox, J., Hein, M.Y., Luber, C.A., Paron, I., Nagaraj, N., and Mann, M. (2014). Accurate proteome-wide label-free quantification by delayed normalization and maximal peptide ratio extraction, termed MaxLFQ. Molecular & cellular proteomics : MCP *13*, 2513-2526. 10.1074/mcp.M113.031591.
42. Tyanova, S., Temu, T., Sinitcyn, P., Carlson, A., Hein, M.Y., Geiger, T., Mann, M., and Cox, J. (2016). The Perseus computational platform for comprehensive analysis of (prote)omics data. Nature methods *13*, 731-740. 10.1038/nmeth.3901.
43. Evans, R., O'Neill, M., Pritzel, A., Antropova, N., Senior, A., Green, T., Žídek, A., Bates, R., Blackwell, S., Yim, J., et al. (2022). Protein complex prediction with AlphaFold-Multimer. bioRxiv, 2021.2010.2004.463034. 10.1101/2021.10.04.463034.
44. Jumper, J., Evans, R., Pritzel, A., Green, T., Figurnov, M., Ronneberger, O., Tunyasuvunakool, K., Bates, R., Zidek, A., Potapenko, A., et al. (2021). Highly accurate protein structure prediction with AlphaFold. Nature *596*, 583-589. 10.1038/s41586-021-03819-2.
45. Mirdita, M., Schutze, K., Moriwaki, Y., Heo, L., Ovchinnikov, S., and Steinegger, M. (2022). ColabFold: making protein folding accessible to all. Nat Methods *19*, 679-682. 10.1038/s41592-022-01488-1.

46. Hornak, V., Abel, R., Okur, A., Strockbine, B., Roitberg, A., and Simmerling, C. (2006). Comparison of multiple Amber force fields and development of improved protein backbone parameters. Proteins *65*, 712-725. 10.1002/prot.21123.
47. Altschul, S.F., Madden, T.L., Schaffer, A.A., Zhang, J., Zhang, Z., Miller, W., and Lipman, D.J. (1997). Gapped BLAST and PSI-BLAST: a new generation of protein database search programs. Nucleic Acids Res *25*, 3389-3402. 10.1093/nar/25.17.3389.
48. Steinegger, M., and Soding, J. (2017). MMseqs2 enables sensitive protein sequence searching for the analysis of massive data sets. Nat Biotechnol *35*, 1026-1028. 10.1038/nbt.3988.
49. McWilliam, H., Li, W., Uludag, M., Squizzato, S., Park, Y.M., Buso, N., Cowley, A.P., and Lopez, R. (2013). Analysis Tool Web Services from the EMBL-EBI. Nucleic Acids Res *41*, W597-600. 10.1093/nar/gkt376.
50. Sievers, F., Wilm, A., Dineen, D., Gibson, T.J., Karplus, K., Li, W., Lopez, R., McWilliam, H., Remmert, M., Soding, J., et al. (2011). Fast, scalable generation of high-quality protein multiple sequence alignments using Clustal Omega. Mol Syst Biol *7*, 539. 10.1038/msb.2011.75.
51. Bailey, T.L., and Elkan, C. (1994). Fitting a mixture model by expectation maximization to discover motifs in biopolymers. Proc Int Conf Intell Syst Mol Biol *2*, 28-36.
52. Croucher, D.R., Rickwood, D., Tactacan, C.M., Musgrove, E.A., and Daly, R.J. (2010). Cortactin modulates RhoA activation and expression of Cip/Kip cyclin-dependent kinase inhibitors to promote cell cycle progression in 11q13-amplified head and neck squamous cell carcinoma cells. Mol Cell Biol *30*, 5057-5070. 10.1128/MCB.00249-10.
53. Bennett, H.L., Brummer, T., Jeanes, A., Yap, A.S., and Daly, R.J. (2008). Gab2 and Src co-operate in human mammary epithelial cells to promote growth factor independence and disruption of acinar morphogenesis. Oncogene *27*, 2693-2704. 10.1038/sj.onc.1210928.
54. Pereira, B., Chin, S.-F., Rueda, O.M., Vollan, H.-K.M., Provenzano, E., Bardwell, H.A., Pugh, M., Jones, L., Russell, R., and Sammut, S.-J. (2016). The somatic mutation profiles of 2,433 breast cancers refine their genomic and transcriptomic landscapes. Nature communications *7*, 11479.
55. Perez-Riverol, Y., Bai, J., Bandla, C., Garcia-Seisdedos, D., Hewapathirana, S., Kamatchinathan, S., Kundu, D.J., Prakash, A., Frericks-Zipper, A., Eisenacher, M., et al. (2022). The PRIDE database resources in 2022: a hub for mass spectrometry-based proteomics evidences. Nucleic Acids Res *50*, D543-D552. 10.1093/nar/gkab1038.

Figure 1.

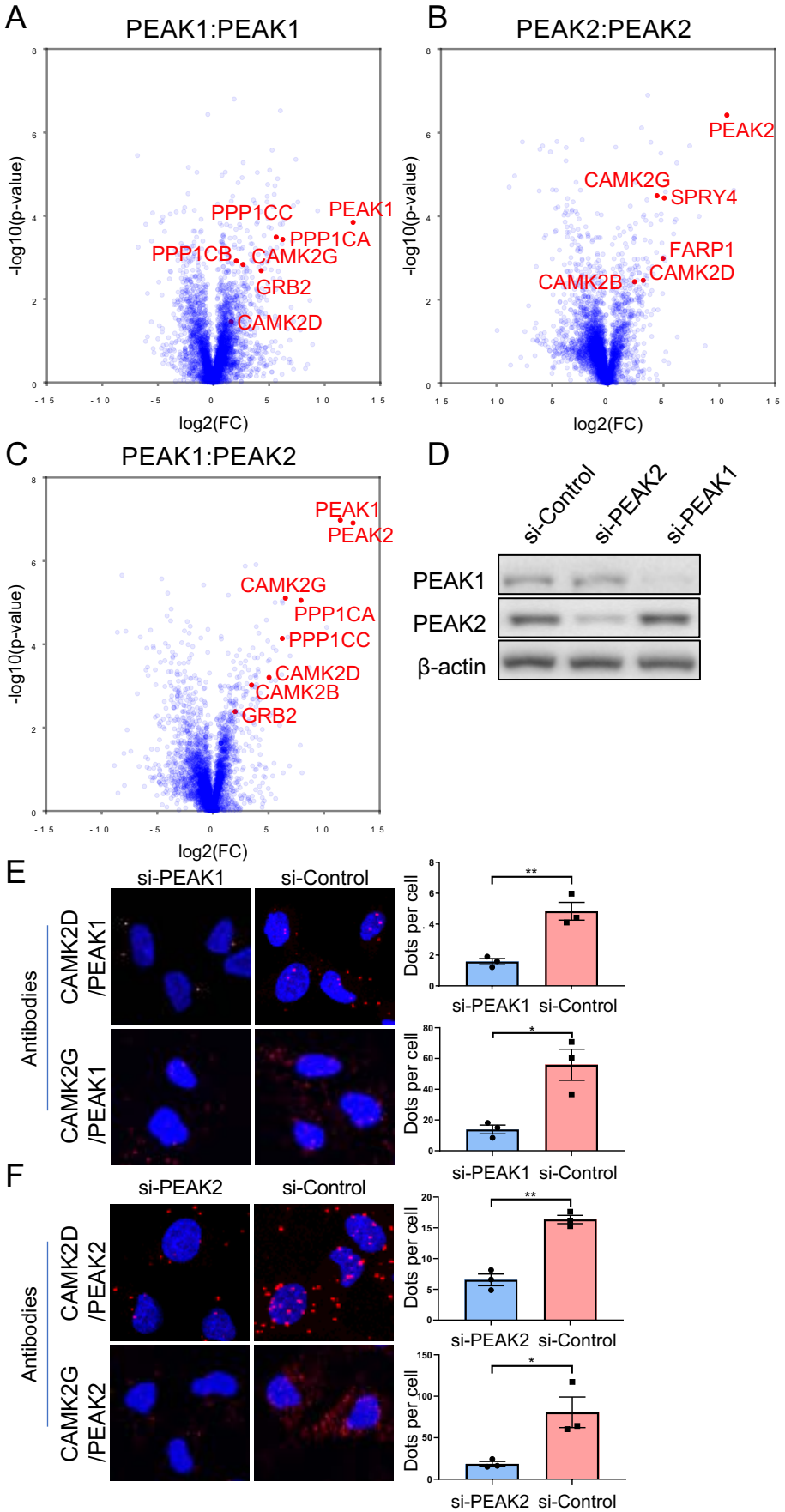
A
PEAK1:PEAK1
-log10(p-value)
log2(FC)
PPP1CC
PEAK1
PPP1CA
PPP1CB
CAMK2G
GRB2
CAMK2D
B
PEAK2:PEAK2
PEAK2
CAMK2G
SPRY4
FARP1
CAMK2D
CAMK2B
C
PEAK1:PEAK2
PEAK1
PEAK2
CAMK2G
PPP1CA
PPP1CC
CAMK2D
CAMK2B
GRB2
D
si-Control
si-PEAK2
si-PEAK1
PEAK1
PEAK2
β-actin
E
si-PEAK1
si-Control
Antibodies
CAMK2D /PEAK1
CAMK2G /PEAK1
Dots per cell
F
si-PEAK2
si-Control
CAMK2D /PEAK2
CAMK2G /PEAK2

Figure 2.

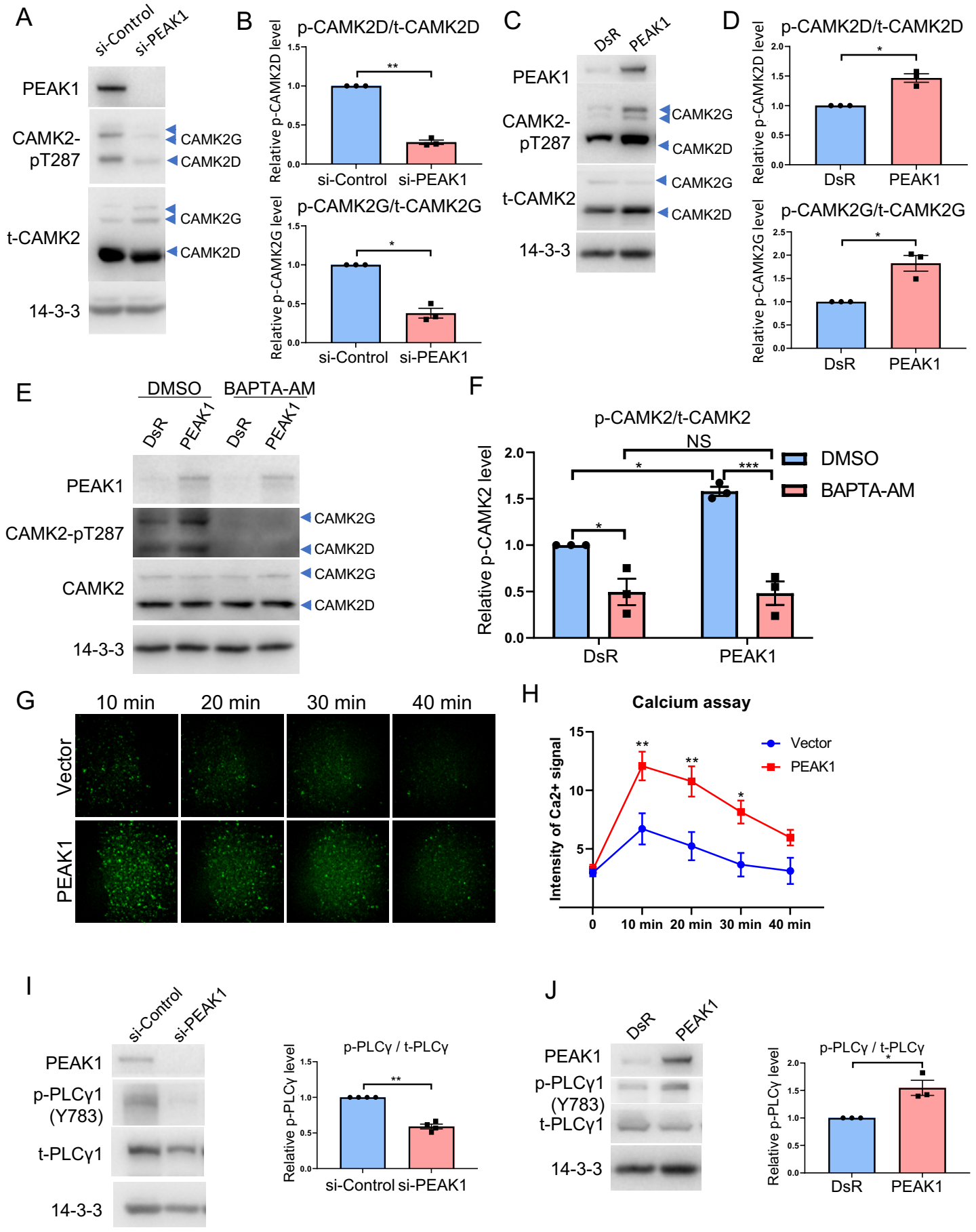
A
si-Control
si-PEAK1
PEAK1
CAMK2-pT287
CAMK2G
CAMK2D
t-CAMK2
CAMK2G
CAMK2D
14-3-3
B
p-CAMK2D/t-CAMK2D
Relative p-CAMK2D level
si-Control
si-PEAK1
p-CAMK2G/t-CAMK2G
Relative p-CAMK2G level
si-Control
si-PEAK1
C
DsR
PEAK1
PEAK1
CAMK2-pT287
CAMK2G
CAMK2D
t-CAMK2
CAMK2G
CAMK2D
14-3-3
D
p-CAMK2D/t-CAMK2D
Relative p-CAMK2D level
DsR
PEAK1
p-CAMK2G/t-CAMK2G
Relative p-CAMK2G level
DsR
PEAK1
E
DMSO
BAPTA-AM
DsR
PEAK1
DsR
PEAK1
PEAK1
CAMK2-pT287
CAMK2G
CAMK2D
CAMK2
CAMK2G
CAMK2D
14-3-3
F
p-CAMK2/t-CAMK2
NS
DMSO
BAPTA-AM
Relative p-CAMK2 level
DsR
PEAK1
G
10 min
20 min
30 min
40 min
Vector
PEAK1
H
Calcium assay
Vector
PEAK1
Intensity of Ca2+ signal
0
10 min
20 min
30 min
40 min
I
si-Control
si-PEAK1
PEAK1
p-PLCγ1 (Y783)
t-PLCγ1
14-3-3
p-PLCγ / t-PLCγ
Relative p-PLCγ level
si-Control
si-PEAK1
J
DsR
PEAK1
PEAK1
p-PLCγ1 (Y783)
t-PLCγ1
14-3-3
p-PLCγ / t-PLCγ
Relative p-PLCγ level
DsR
PEAK1

Figure 3.

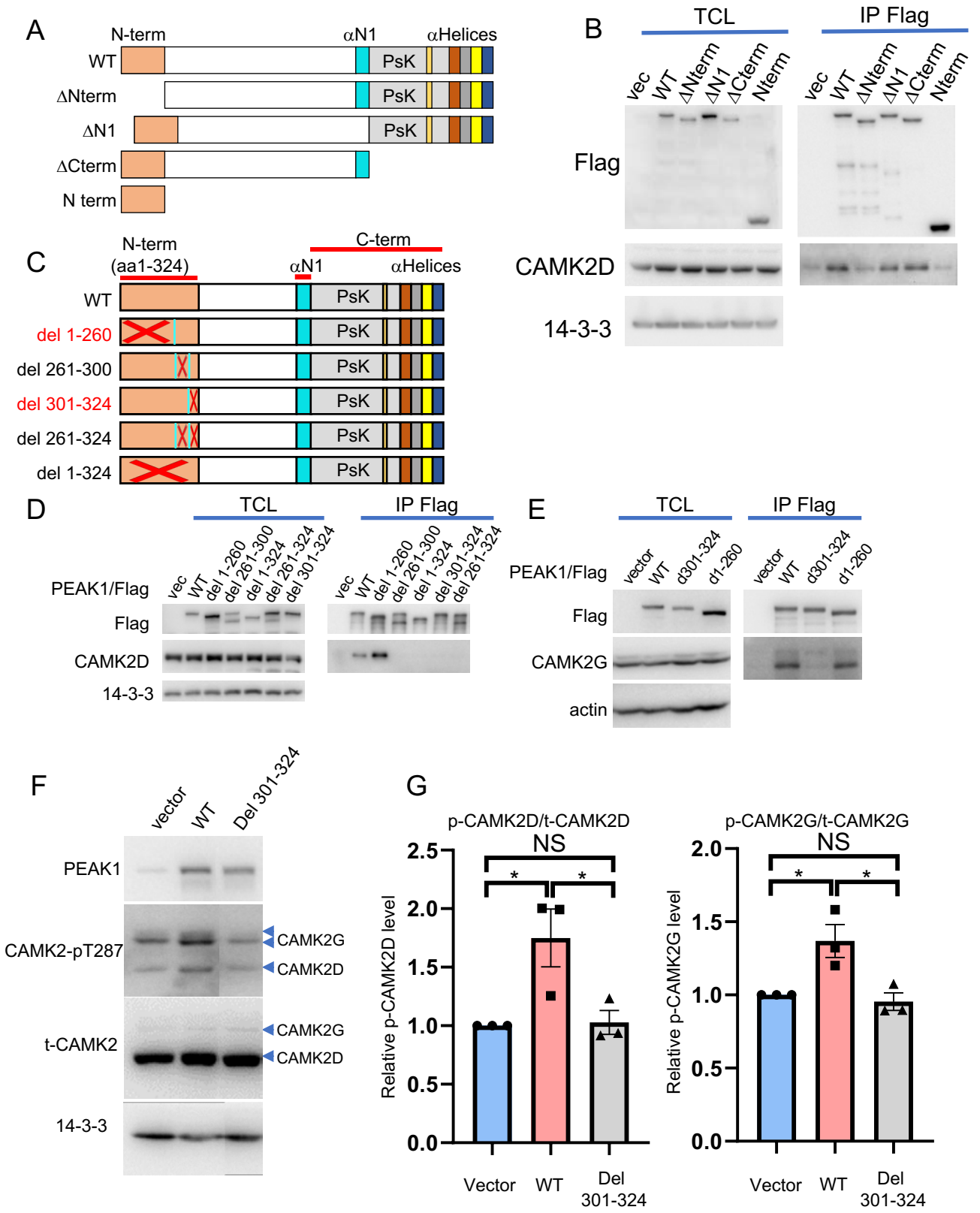
A
N-term
αN1
αHelices
WT
PsK
ΔNterm
ΔN1
ΔCterm
N term
B
TCL
IP Flag
vec
WT
ΔNterm
ΔN1
ΔCterm
Nterm
Flag
CAMK2D
14-3-3
C
N-term
(aa1-324)
C-term
αN1
αHelices
del 1-260
del 261-300
del 301-324
del 261-324
del 1-324
D
TCL
IP Flag
PEAK1/Flag
del 1-260
del 261-300
del 1-324
del 261-324
del 301-324
Flag
CAMK2D
14-3-3
E
TCL
IP Flag
vector
d301-324
d1-260
CAMK2G
actin
F
vector
WT
Del 301-324
PEAK1
CAMK2-pT287
CAMK2G
CAMK2D
t-CAMK2
14-3-3
G
p-CAMK2D/t-CAMK2D
NS
Relative p-CAMK2D level
Vector
WT
Del
301-324
p-CAMK2G/t-CAMK2G
Relative p-CAMK2G level

Figure 4.

A

									-8					-5					-3					0	
GluN2B	-	-	-	-	-	-	-	-	R	-	N	K	-	L	-	-	R	-	R	Q	-	H	S	Y	D
Tiam1	R	T	L	D	S	H	A	S	R	M	T	Q	-	L	-	-	K	-	K	Q	-	A	A	L	-
densin-180	-	-	-	-	-	S	H	G	R	-	R	P	-	L	-	-	I	-	R	Q	D	R	I	V	G
GluA1	-	-	-	-	S	K	R	M	K	G	F	C	-	L	-	-	I	-	P	Q	-	Q	S	I	N
CAMKIIN	-	-	-	-	-	-	-	K	R	-	P	P	K	L	G	Q	I	G	R	S	-	K	R	V	V
PEAK1	K	K	W	N	T	I	P	L	R	-	N	K	S	L	-	Q	-	-	R	I	-	C	A	V	D
									R297					L301					R303						

B

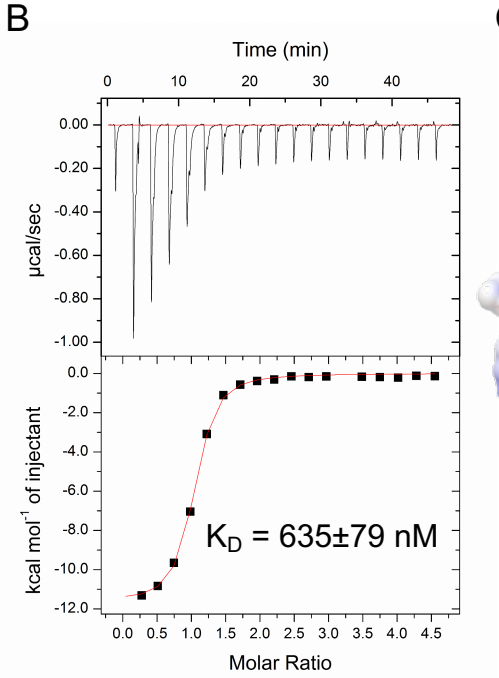

C

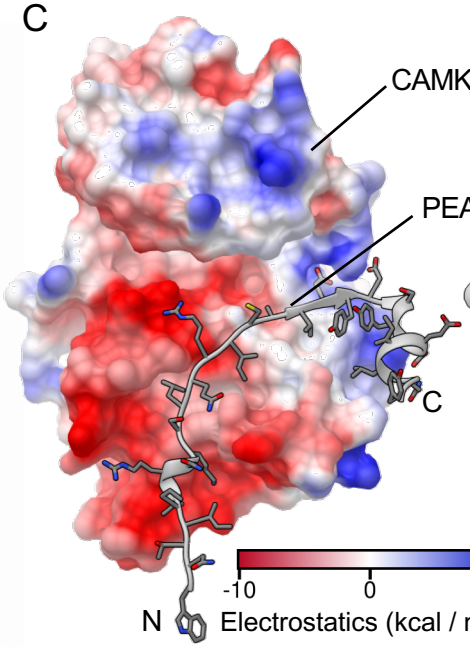

D

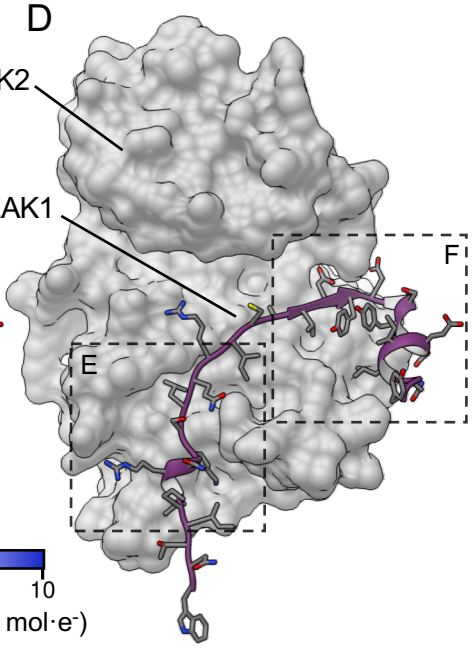

E

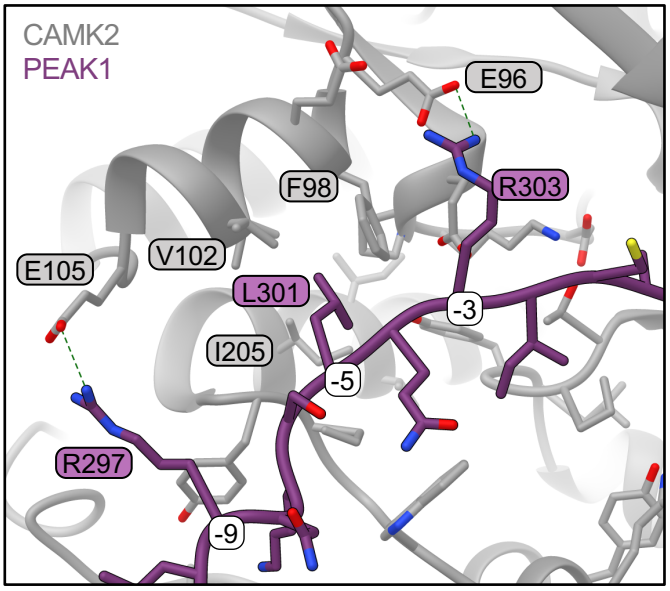

F

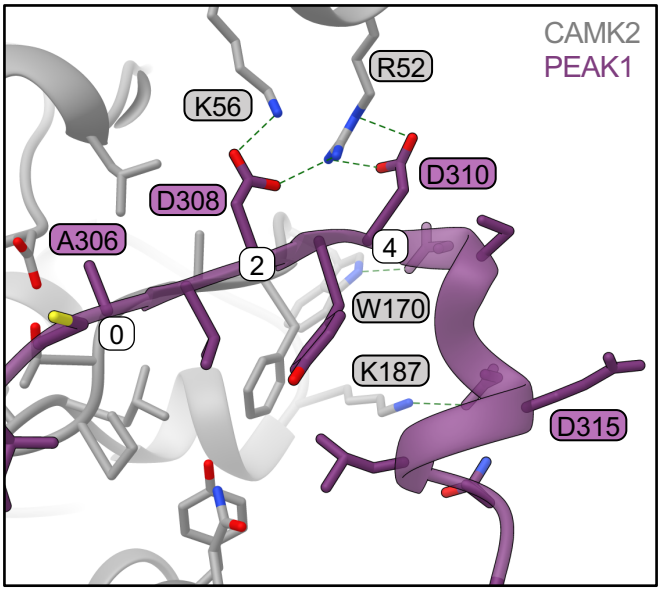

Figure 5.

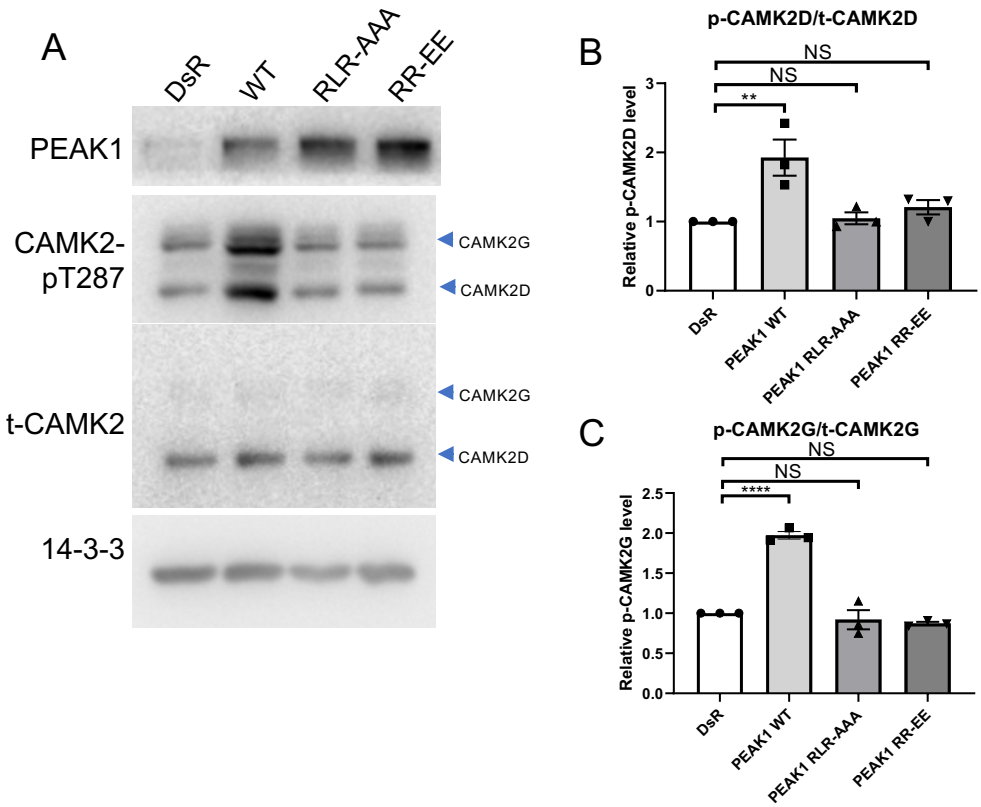
A
DsR
WT
RLR-AAA
RR-EE
PEAK1
CAMK2-
pT287
CAMK2G
CAMK2D
t-CAMK2
CAMK2G
CAMK2D
14-3-3
B
p-CAMK2D/t-CAMK2D
NS
NS
**
Relative p-CAMK2D level
0
1
2
3
DsR
PEAK1 WT
PEAK1 RLR-AAA
PEAK1 RR-EE
C
p-CAMK2G/t-CAMK2G
NS
NS
****
Relative p-CAMK2G level
0.0
0.5
1.0
1.5
2.0
2.5
DsR
PEAK1 WT
PEAK1 RLR-AAA
PEAK1 RR-EE

Figure 6.

A

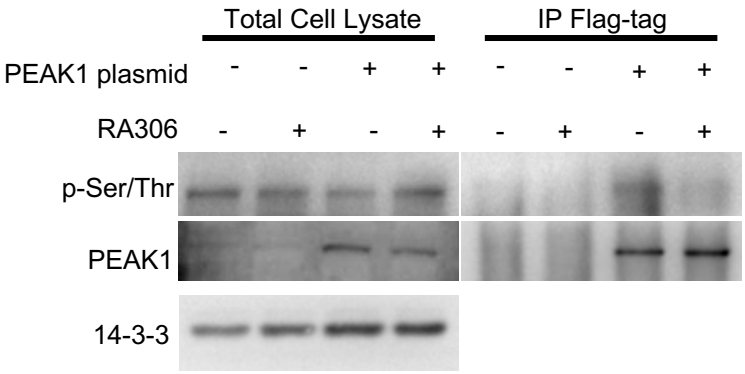

B

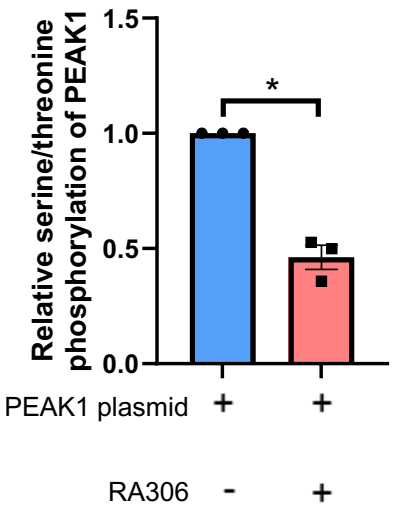

C

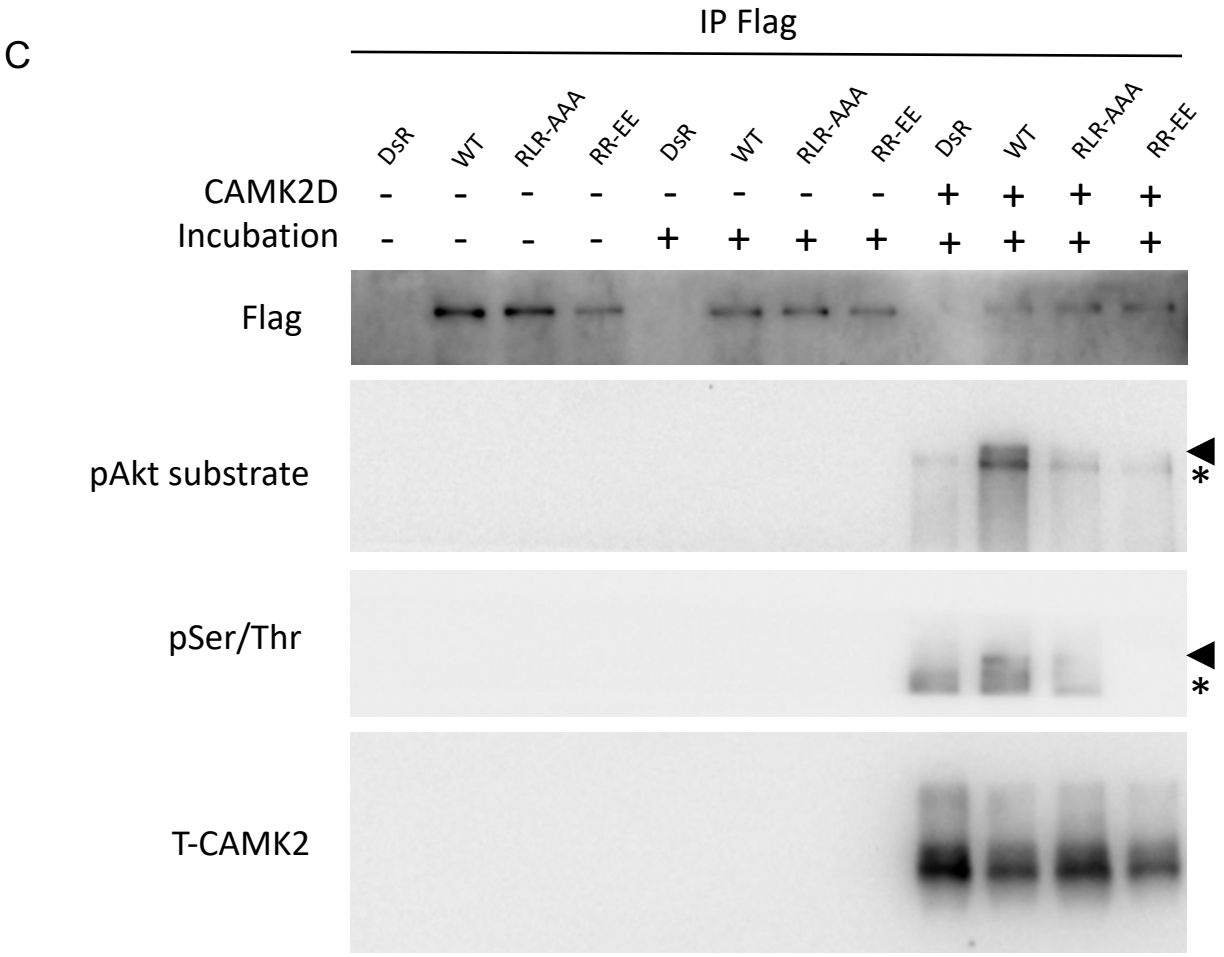

D

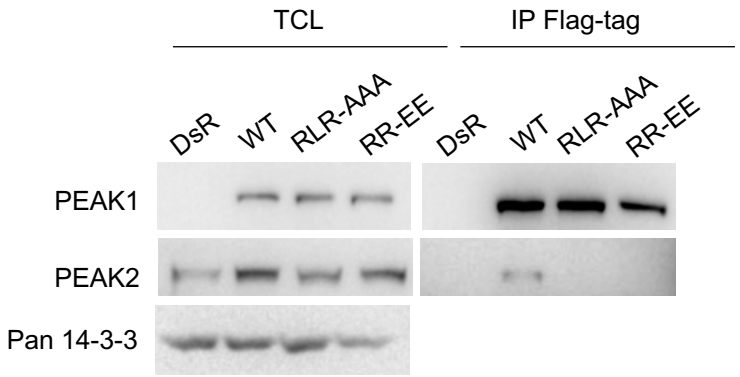

Figure 7.

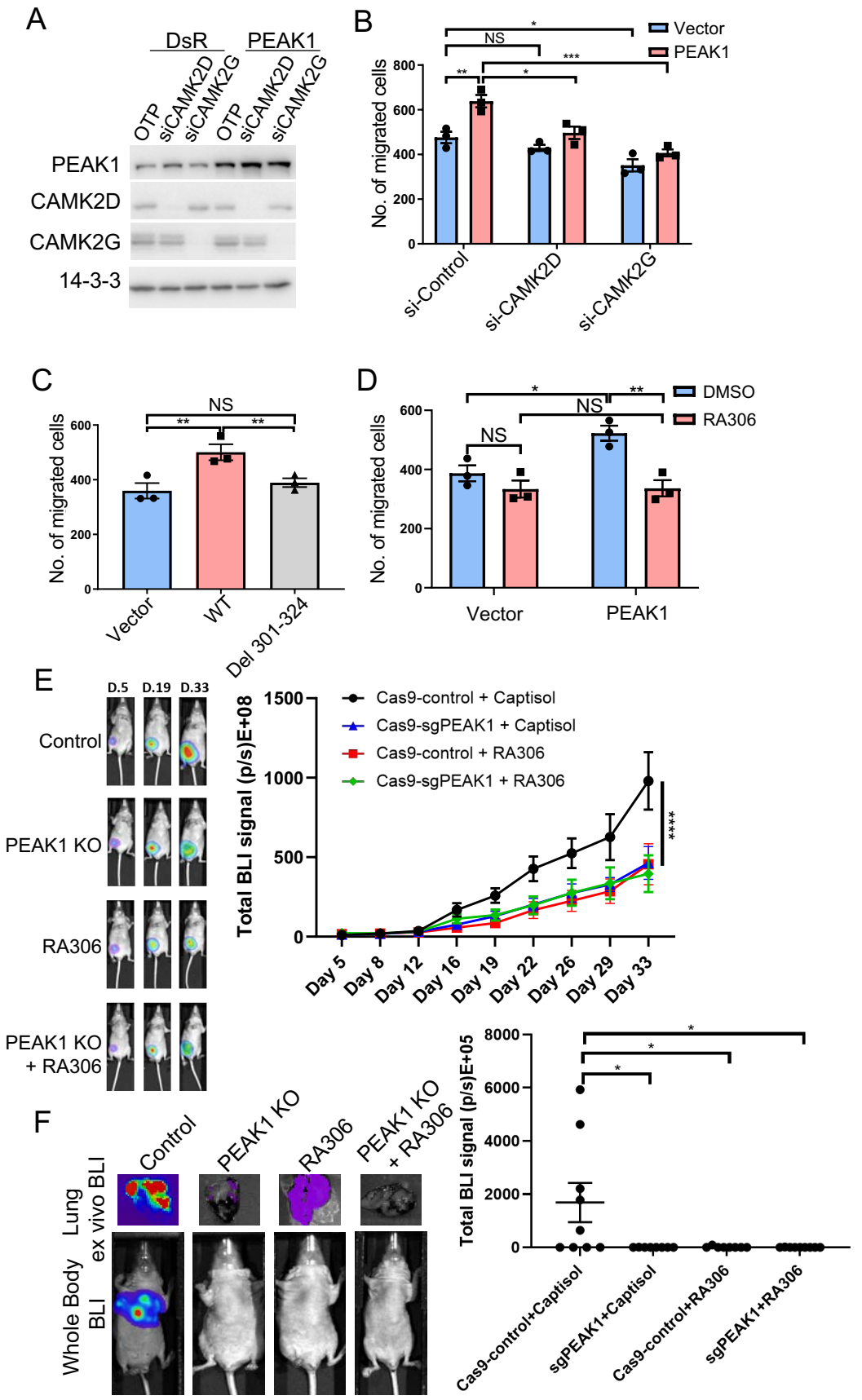
A
DsR
PEAK1
OTP
siCAMK2D
siCAMK2G
OTP
siCAMK2D
siCAMK2G
PEAK1
CAMK2D
CAMK2G
14-3-3
B
Vector
PEAK1
No. of migrated cells
si-Control
si-CAMK2D
si-CAMK2G
C
No. of migrated cells
Vector
WT
Del 301-324
D
DMSO
RA306
No. of migrated cells
Vector
PEAK1
E
D.5
D.19
D.33
Control
PEAK1 KO
RA306
PEAK1 KO
+ RA306
Cas9-control + Captisol
Cas9-sgPEAK1 + Captisol
Cas9-control + RA306
Cas9-sgPEAK1 + RA306
Total BLI signal (p/s)E+08
Day 5
Day 8
Day 12
Day 16
Day 19
Day 22
Day 26
Day 29
Day 33
F
Control
PEAK1 KO
RA306
PEAK1 KO
+ RA306
Lung
ex vivo BLI
Whole Body
BLI
Total BLI signal (p/s)E+05
Cas9-control+Captisol
sgPEAK1+Captisol
Cas9-control+RA306
sgPEAK1+RA306

Supplementary Figures

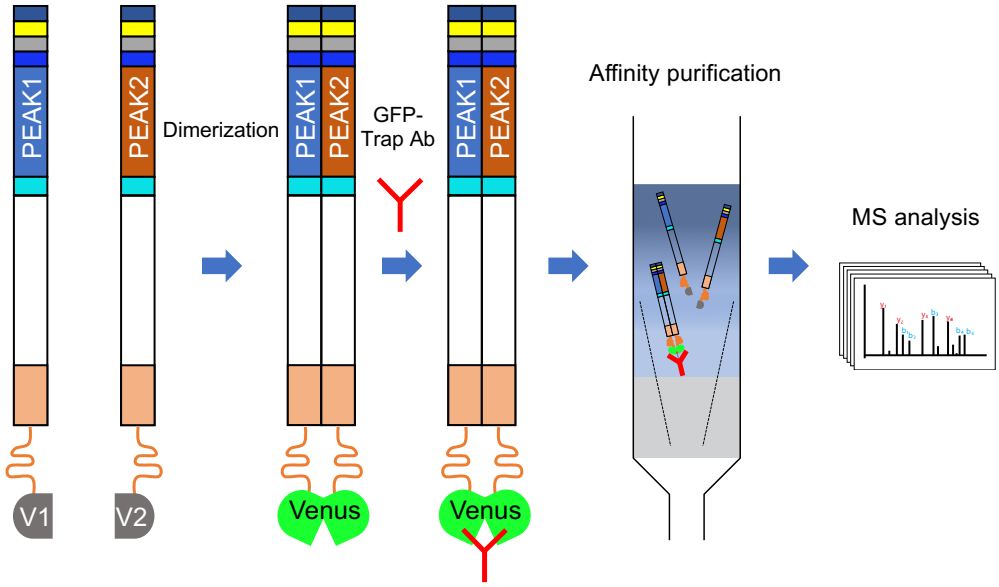

Supp. Figure 1. Schematic strategy of BiCAP-MS/MS screen. This is indicated for the PEAK1/PEAK2 heterodimer. PEAK1 and PEAK2 were fused to N-terminal (V1) and C-terminal (V2) fragments of the Venus protein, respectively. When PEAK1 and PEAK2 associate, V1 and V2 bind to each other and reconstitute Venus that can be recognized by the GFP-targeting nanobody (GFP-Trap). The heterodimer and its interactome can then be immunoaffinity purified for MS analysis. In the screen, this workflow was applied to the PEAK1 and PEAK2 homodimers as well as the heterodimer.

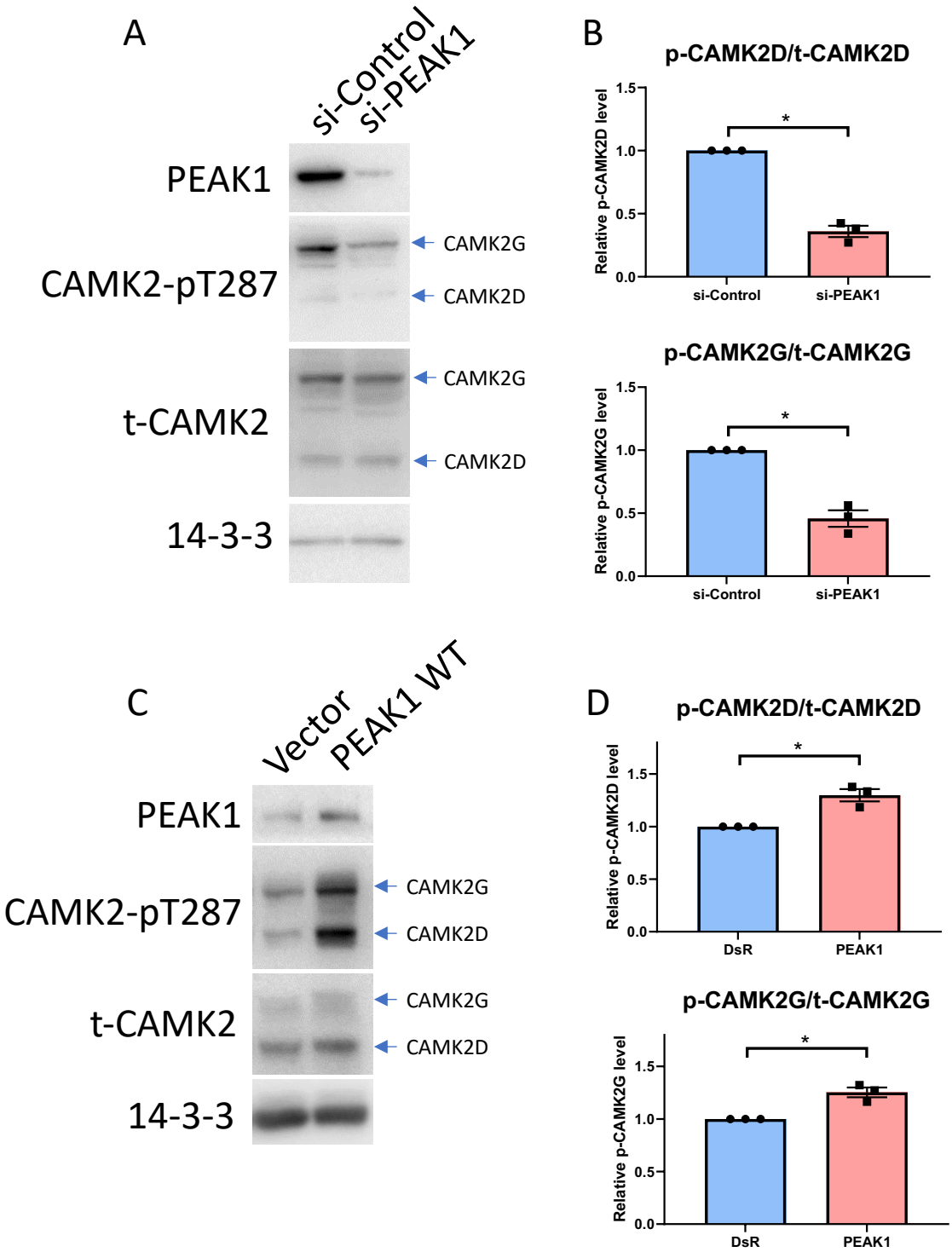

Supp. Figure 2. Manipulation of PEAK1 expression modulates CAMK2 activity in MDA-MB-468 cells. PEAK1 was knocked down using siRNA (A-B) or overexpressed via transient transfection (C-D) in MDA-MB-468 cells and autonomous activation of CAMK2 determined by Western blotting as indicated. Histograms indicate CAMK2 T287 phosphorylation normalized for total CAMK2 expression. * = $p < 0.05$, ** = $p < 0.01$, *** = $p < 0.001$ by ratio paired t-test.

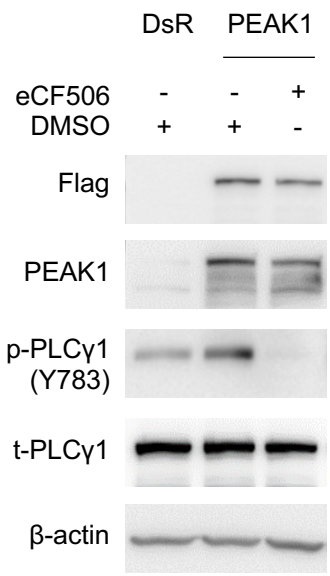

Supp. Figure 3. Effect of SFK inhibitor eCF506 on PLCγ1 Y783 phosphorylation. MDA-MB-231_EcoR cells stably transduced with DsR empty vector or the corresponding PEAK1 construct were treated with DMSO or the SFK inhibitor eCF506 (250 nM) for 1 h. Cell lysates were then analysed by Western blotting as indicated. Data are representative of replicate experiments.

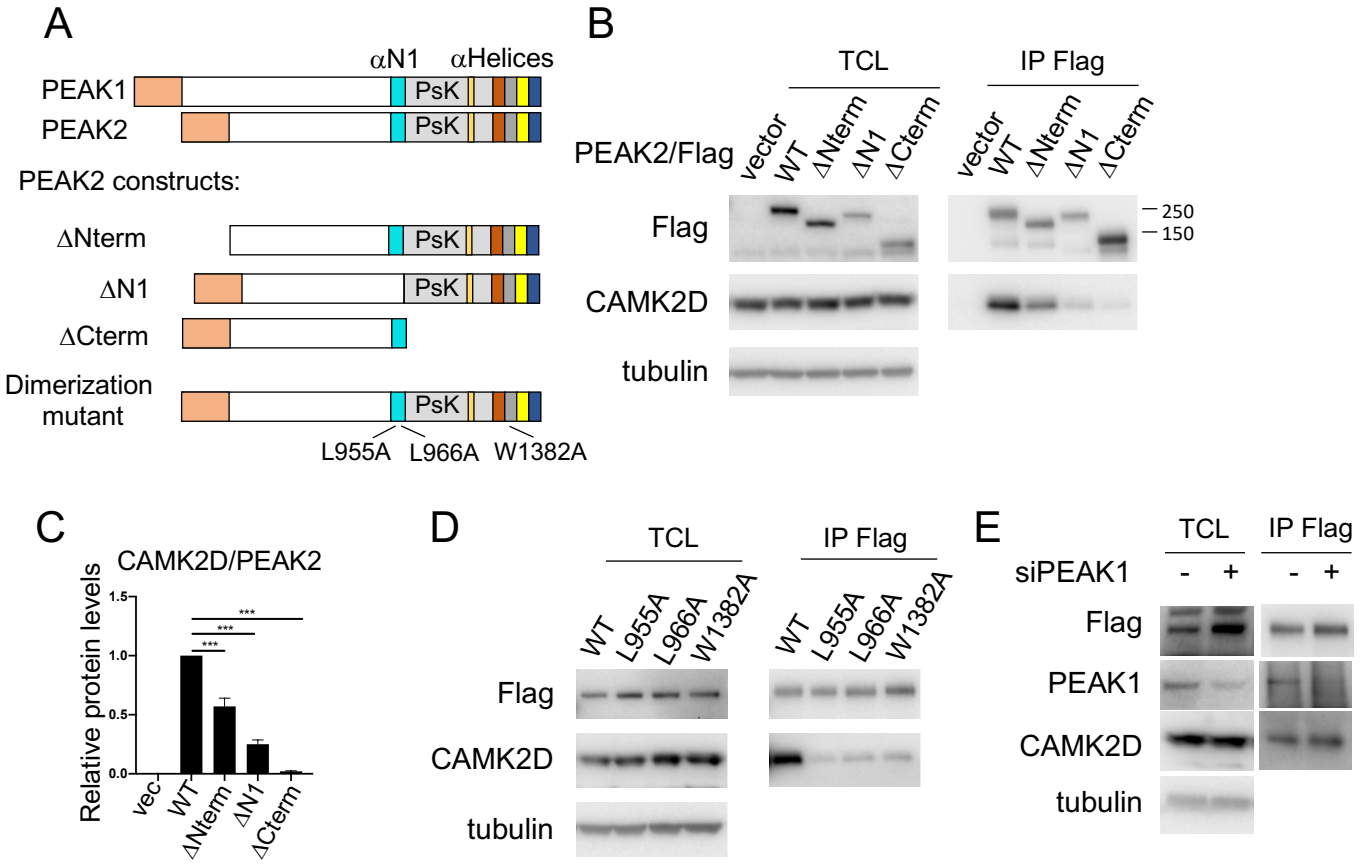

Supp. Figure 4. Determination of the structural requirements for CAMK2 interaction with PEAK2. A. Schematic structure of PEAK2 and various deletion and point mutants. **B. Identification of PEAK2 regions required for association with CAMK2D.** Flag-tagged versions of the indicated PEAK2 proteins were transfected into HEK293T cells. Total cell lysates (TCL) and Flag immunoprecipitates (IPs) were subjected to Western blotting. **C. Quantification of CAMK2D association.** CAMK2D binding to PEAK2 was quantified and normalized for the PEAK2 level. Data are expressed relative to WT which was arbitrarily set at 1. **D. Role of PEAK2 dimerization in regulating association with CAMK2D.** Flag-tagged versions of the indicated PEAK2 proteins were expressed in HEK293T cells. TCL and Flag IPs were subjected to Western blotting as indicated. **E. The association of PEAK2 with CAMK2D is PEAK1-independent.** HEK293T cells were transfected with a plasmid encoding Flag-tagged PEAK2 in the presence or absence of siRNA-mediated PEAK1 knockdown. TCL and Flag IPs were subjected to Western blotting as indicated. All data are representative of at least 2 independent experiments. Error bars in C represent the standard error of the mean from n=3 independent experiments. *** = $p < 0.001$ by one-way ANOVA with Dunnett's multiple comparisons test.

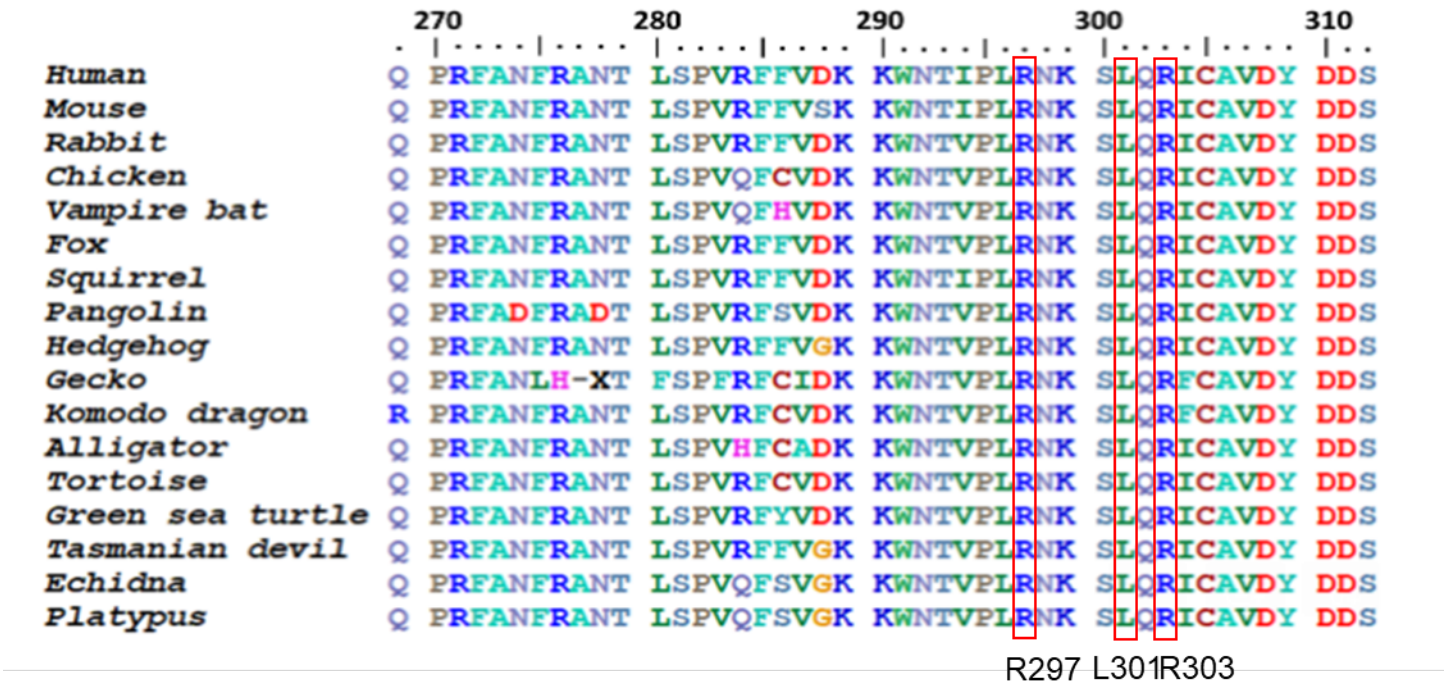

Supp. Figure 5. Sequence alignment of the PEAK1 CIM motif across diverse species. The critical residues for CAMK2 interaction, R297, L301 and R303 are conserved across species and highlighted in red boxes.

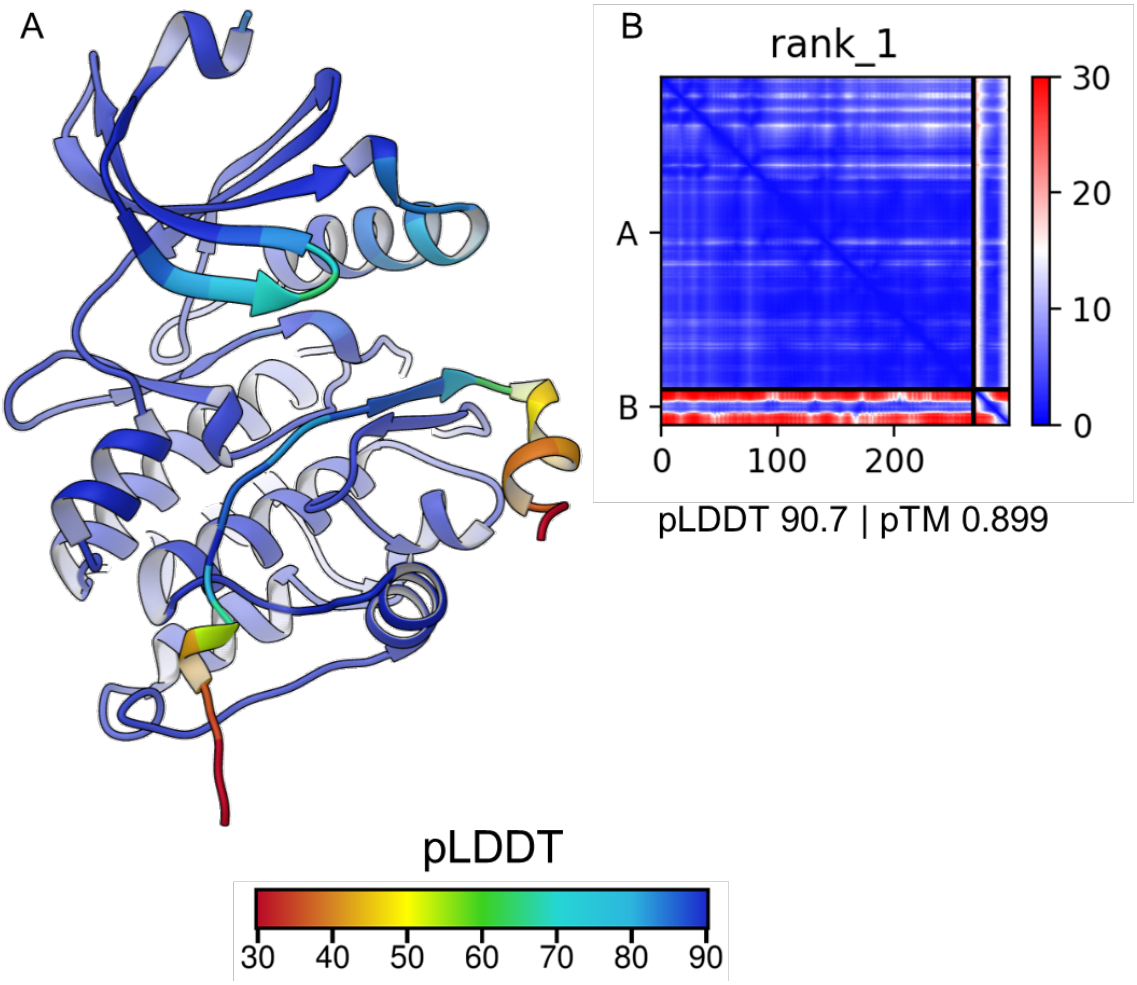

Supp. Figure 6. Comparative modelling analysis by AlphaFold (to accompany Figure 4C-F). A. Computationally predicted PEAK1(291-320)/CAMK2 model by AlphaFold (v3) coloured according to pLDDT score. Overall pLDDT and pTM scores of 90.7 and 0.899 indicate high estimated confidence measured by per-residue local distance difference (LDDT) and residue-residue alignment error estimate respectively. **B. Predicted alignment error plot illustrating low overall estimated error between PEAK1(291-320) and CaMK2 (top right quadrant).**

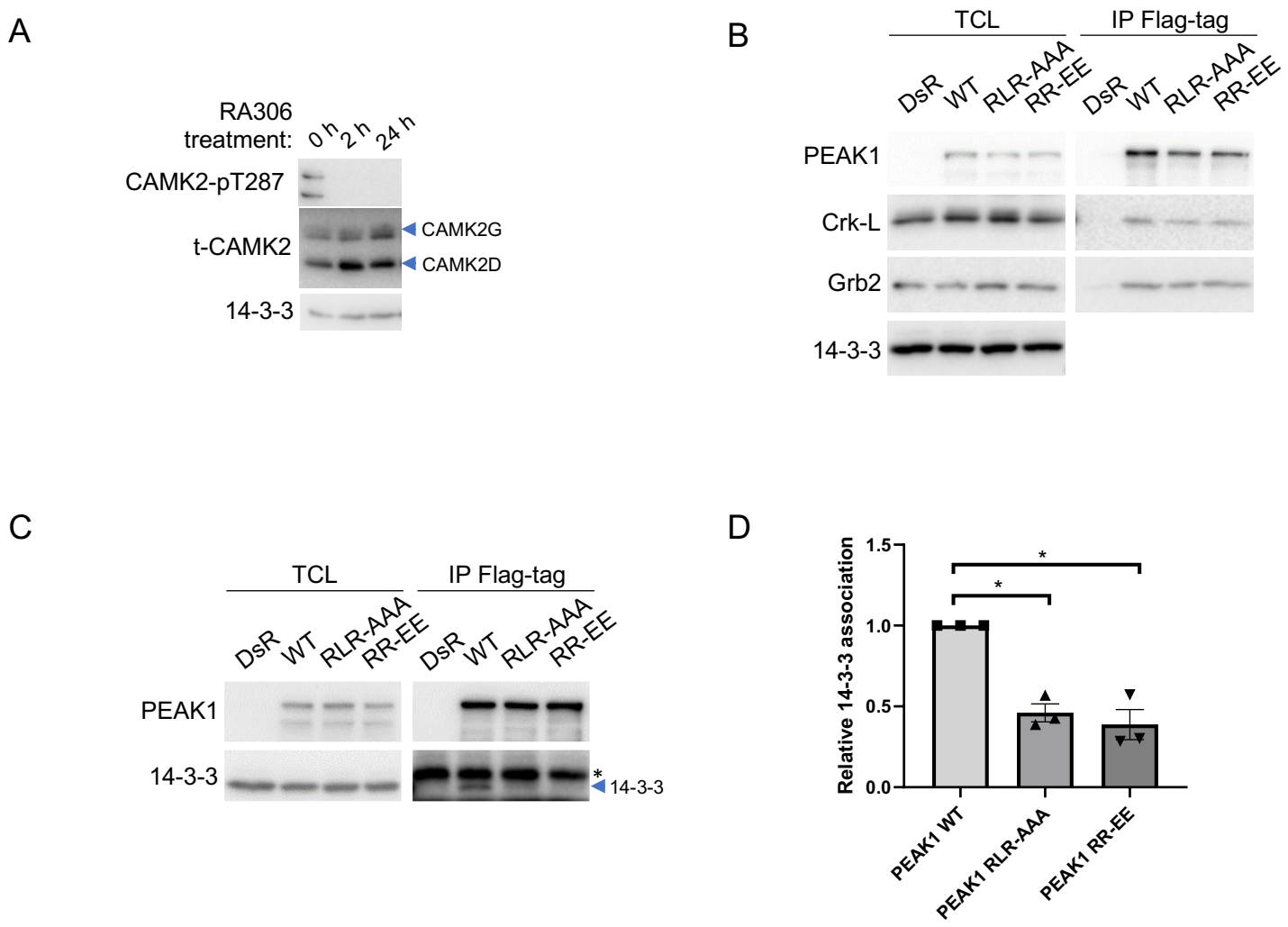

Supp. Figure 7. Role of CAMK2 in regulating PEAK1 phosphorylation and the PEAK1 interactome. A. Validation of CAMK2 inhibition using RA306. MDA-MB-231 cells were treated with 1 μM RA306 for the specified times and then cell lysates were Western blotted as indicated. Data are representative of triplicate experiments. **B-D. Impact of CIM mutations on the PEAK1 interactome.** IPs of WT and mutant PEAK1 proteins from HEK293T cells were analysed by immunoblotting with the indicated antibodies. Results are representative of 3 independent experiments. The asterisk in C indicates a non-specific band. Histogram (D) indicates the association of 14-3-3 relative to WT PEAK1 (mean ± s.e.m., n = 3). * = $p < 0.05$ by ratio t-test.

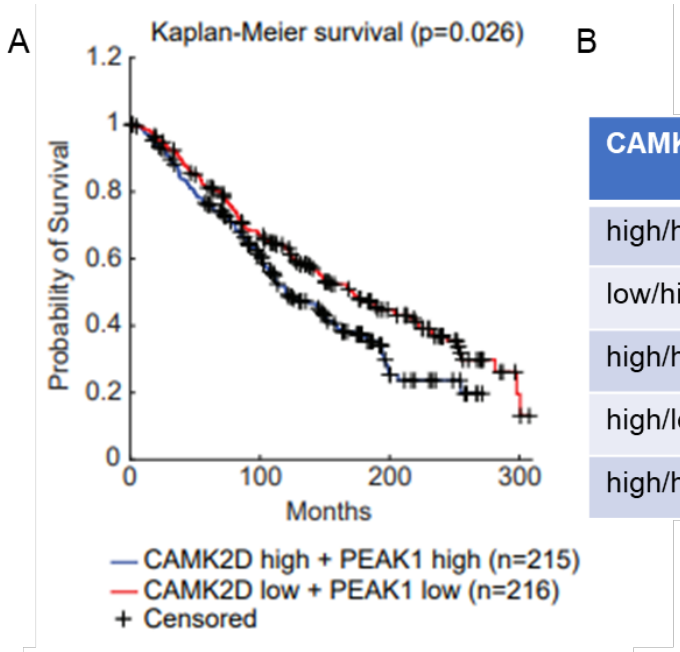

B

Comparison

CAMK2D/PEAK1	CAMK2D/PEAK1	P-value
high/high	low/low	**0.026**
low/high	low/low	**0.8**
high/high	high/low	**0.051**
high/low	low/low	0.71
high/high	low/high	**0.026**

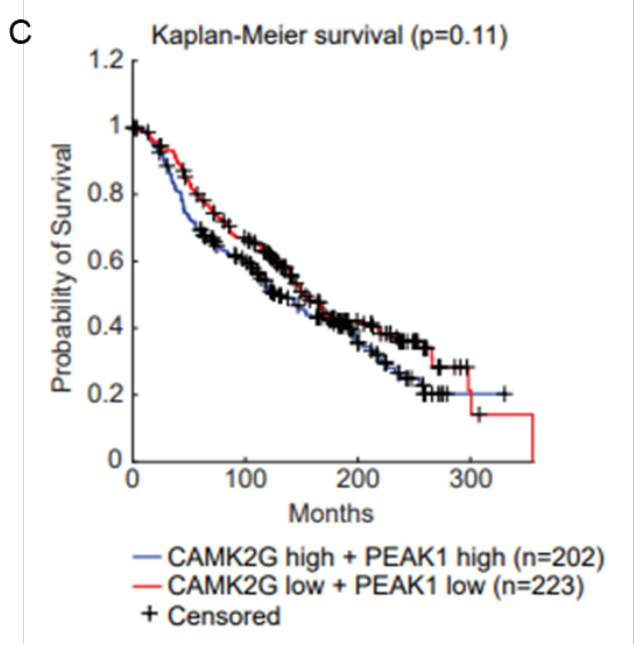

Supp. Figure 8. Association of PEAK1 and CAMK2 expression with breast cancer patient survival. Gene expression, mutation profile and associated overall survival data from 2509 breast cancer patients were downloaded from the cBioPortal for Cancer Genomics portal (https://www.cbioportal.org/). Breast cancer patients were categorised into groups exhibiting different PEAK1/CAMK2 combined expression patterns. **A. Survival analyses comparing overall survival between PEAK1/CAMK2D both high and PEAK1/CAMK2D both low.** This was undertaken using a Log-rank test. **B. Summary table comparing overall survival differences between indicated PEAK1/CAMK2D combined expression patterns. C. Survival analyses comparing overall survival between PEAK1/CAMK2G both high and PEAK1/CAMK2G both low.** The Log-rank test statistics and survival curves were generated using Kaplan-

Meier estimate and implemented using the Logrank package in MATLAB 2023a (with $p < 0.05$ considered significant).

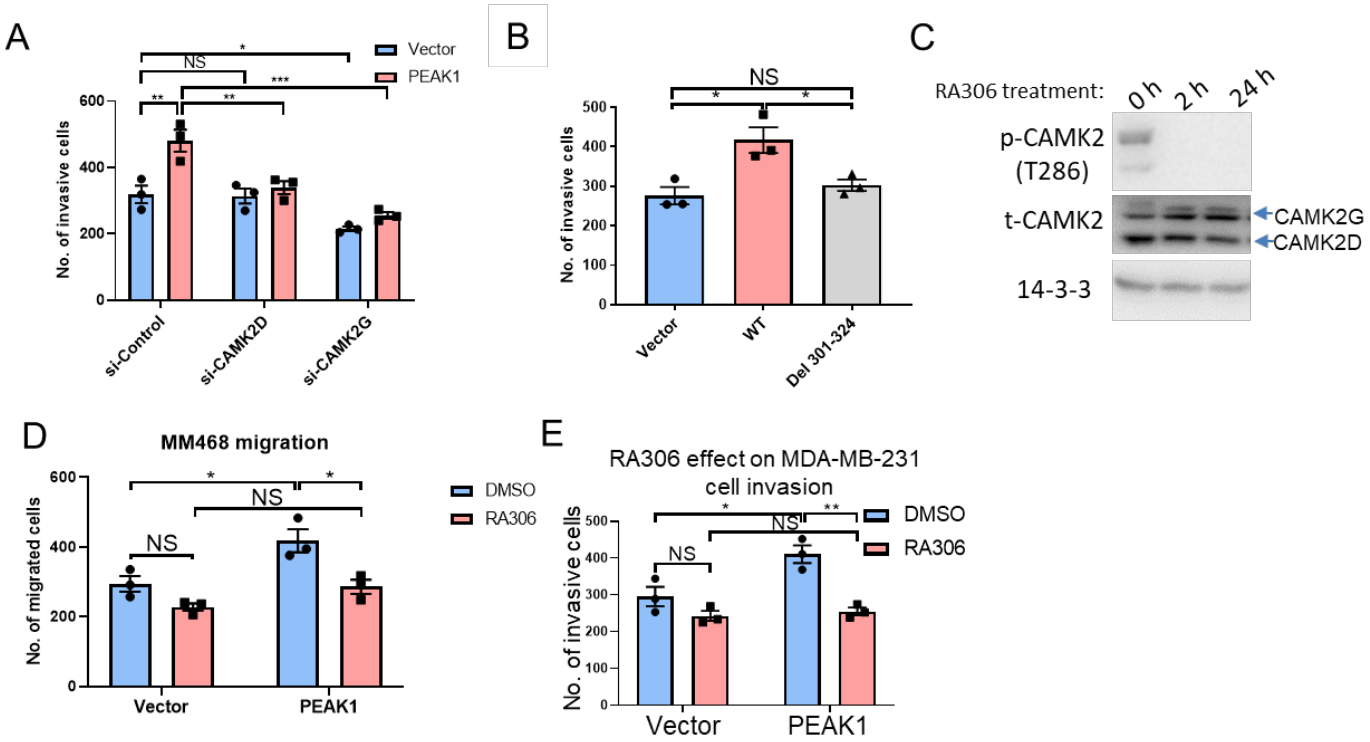

Supp. Figure 9. Role of CAMK2 in PEAK1-regulated biological endpoints in TNBC models. A. Role of CAMK2D/G in PEAK1-promoted MDA-MB-231 cell invasion. MDA-MB-231 cells were transfected with a PEAK1 expression plasmid in the presence or absence of siRNA-mediated CAMK2D or CAMK2G knockdown. Cell lysates were validated by Western blotting in Figure 7A. Cells were subjected to a transwell invasion assay. **B. Role of CAMK2 activation.** Plasmids expressing WT PEAK1 and the del 301-324 mutant that cannot activate CAMK2 were transiently transfected into MDA-MB-231 cells, and cells were subjected to a transwell invasion assay. **C-E. Pharmacological inhibition of CAMK2 using RA306 blocks PEAK1-promoted TNBC cell migration and invasion.** MDA-MB-468 cells were treated with RA306 for different times and cell lysates were then Western blotted as indicated (C). MDA-MB-468 cells were transfected with a PEAK1 plasmid and subject to transwell migration assays in the presence or absence of RA306 (D). MDA-MB-231 cells were transfected with a PEAK1 plasmid and subjected to transwell invasion assays in the presence or absence of RA306 (E). Error bars represent the standard error of the mean from n=3 independent assays. NS indicates $p > 0.05$, * = $p < 0.05$, ** = $p < 0.01$, *** = $p < 0.001$ by two-way ANOVA with Tukey's multiple comparisons test (A, D, E) or one-way ANOVA with Tukey's multiple comparisons test (B).

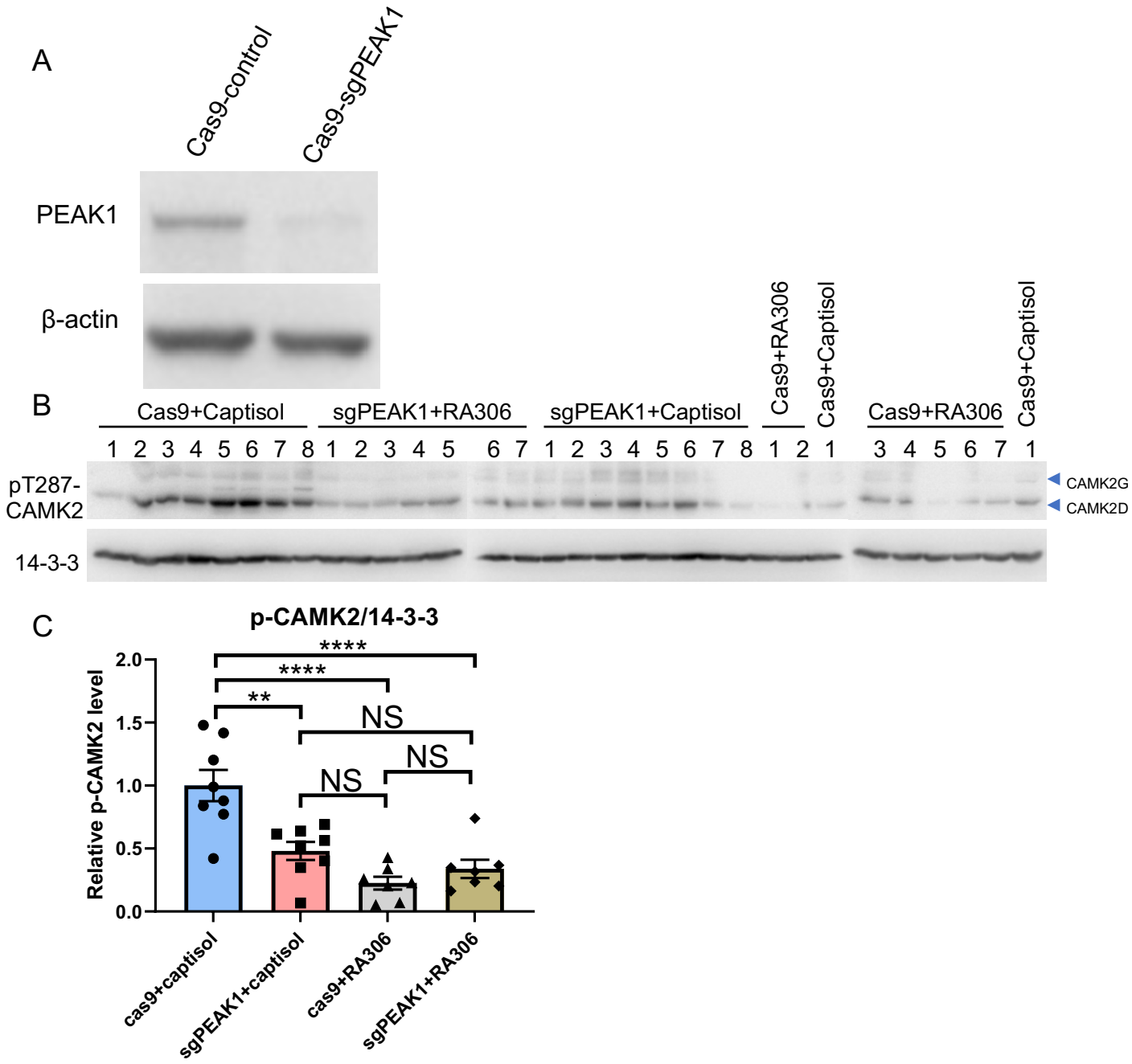

Supp. Figure 10. Genetic or pharmacological targeting of the PEAK1/CAMK2 axis reduces TNBC development *in vivo*. A. Validation of CRISPR-mediated PEAK1 knockout in MDA-MB-231_HM cells. Cells were Western blotted as indicated. **B-C. CAMK2 activation in different xenograft treatment groups.** Tumour tissue from each group was harvested at 2 h after last RA306 treatment, homogenized and subjected to Western blotting (B) and quantification for combined CAMK2D and CAMK2G activation (C) as indicated. In C, data are expressed relative to Cas9-control/Captisol which was arbitrarily set at 1. Error bars represent the standard error of the mean. NS indicates $p > 0.05$, ** = $p < 0.01$, **** = $p < 0.0001$ by two-way ANOVA with Tukey's multiple comparisons test.

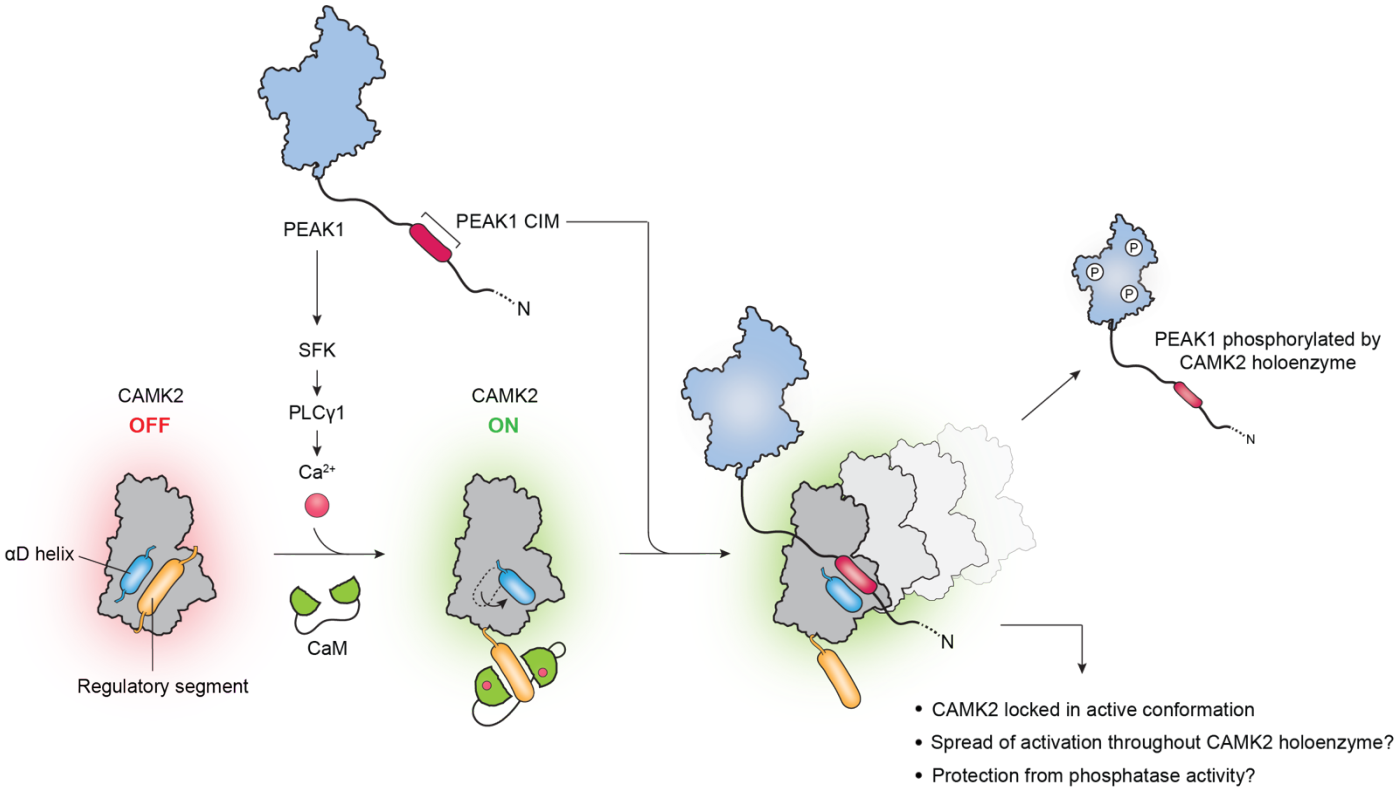

Supp. Figure 11. Schematic representation of feed-forward regulation of CAMK2 by PEAK1. PEAK1 enhances intracellular Ca^{2+} by promoting SFK-mediated tyrosine phosphorylation of PLCγ1. This leads to classical activation of CAMK2 by Ca^{2+}/CaM and the αD helix rotates out. The PEAK1 CIM then binds to the CAMK2 substrate binding site and competes with the regulatory segment, effectively 'locking' CAMK2 in an active conformation. Sustained phosphorylation of PEAK1 and CAMK2 itself (on T287) then occurs as the PEAK1 CIM undergoes cycles of dissociation and re-association. However, other mechanisms may contribute to the observed effects on CAMK2 activation, as indicated on the figure. CIM-mediated recruitment of PEAK1 to the CAMK2 holoenzyme promotes serine/threonine phosphorylation of PEAK1 which in turn positively regulates heterotypic association with PEAK2.